Journal of Human Evolution 173 (2022) 103265

Contents lists available at ScienceDirect

Journal of Human Evolution

journal homepage: www.elsevier.com/locate/jhevol

Comparative description and taxonomic affinity of 3.7-million-year-old hominin mandibles from Woranso-Mille (Ethiopia)

Yohannes Haile-Selassie [a, *], Beverly Z. Saylor [b], Mulugeta Alene [c], Alan Deino [d], Luis Gibert [e], Gary T. Schwartz [a]

[a] Institute of Human Origins and School of Human Evolution and Social Change, Arizona State University, Tempe, AZ, USA
[b] Department of Earth, Environmental and Planetary Sciences, Case Western Reserve University, Cleveland, OH, USA
[c] School of Earth Sciences, Addis Ababa University, Addis Ababa, Ethiopia
[d] Berkeley Geochronology Center, Berkeley, CA, USA
[e] Departament de Mineralogia, Petrologia i Geologia Aplicada, Facultat de Ciències de la Terra, Universitat de Barcelona, Barcelona, Spain

ARTICLE INFO

Article history:
Received 6 December 2021
Accepted 2 September 2022
Available online 25 October 2022

Keywords:
Taxonomy
Australopithecus anamensis
Australopithecus afarensis
Kanapoi
Hadar
Laetoli

ABSTRACT

Fossil discoveries of early *Australopithecus* species from Woranso-Mille have played a significant role in improving our understanding of mid-Pliocene hominin evolution and diversity. Here, we describe two mandibles with dentitions, recovered from sediments immediately above a tuff radiometrically dated to 3.76 ± 0.02 Ma, and assess their taxonomic affinity. The two mandibles (MSD-VP-5/16 and MSD-VP-5/50) show morphological similarities with both *Australopithecus anamensis* and *Australopithecus afarensis*. Some of the unique features that distinguish *Au. anamensis* from *Au. afarensis* are present in the mandibles, which also share a few derived features with *Au. afarensis*. Their retention of more Kanapoi *Au. anamensis*-like traits, compared to the fewer derived features they share with *Au. afarensis*, and the presence of *Au. anamensis* at Woranso-Mille in 3.8-million-year-old deposits, lends support to their assignment to *Au. anamensis*. However, it is equally arguable that the few derived dentognathic features they share with *Au. afarensis* could be taxonomically more significant, making it difficult to conclusively assign these specimens to either species. Regardless of which species they are assigned to, the mosaic nature of the dentognathic morphology and geological age of the two mandibles lends further support to the hypothesized ancestor–descendant relationship between *Au. anamensis* and *Au. afarensis*. However, there is now limited fossil evidence indicating that these two species may have overlapped in time. Hence, the last appearance of *Au. anamensis* and first appearance of *Au. afarensis* are currently unknown. Recovery of *Australopithecus* fossils from 4.1 to 3.8 Ma is critical to further address the timing of these events.

1. Introduction

Hominin fossil discoveries during the last three decades have redefined our understanding of the tempo and mode of human evolution during the Plio-Pleistocene (Brunet et al., 1996, 2002; Leakey et al., 2001; Alemseged et al., 2006, 2020; White et al., 2006; Berger et al., 2010, 2015; Haile-Selassie et al., 2010a, 2010b, 2012, 2015, 2019; Villmoare et al., 2015; Herries et al., 2020). The discovery of the earliest known fossil of the *Homo* lineage at 2.8 Ma, in the Afar region of Ethiopia (Villmoare et al., 2015; DiMaggio et al., 2015), the recognition of different hominin species contemporaneous with *Australopithecus afarensis* from the mid-Pliocene period in eastern and central Africa (*Australopithecus bahrelghazali*, *Kenyanthropus platyops*, *Australopithecus deyiremeda*; Brunet et al., 1996; Leakey et al., 2001; Spoor et al., 2010, 2016; Haile-Selassie et al., 2012, 2015), and recent fossil discoveries of previously known species such as *Australopithecus anamensis* (Haile-Selassie et al., 2019), have challenged several long-held ideas and hypotheses about early hominin taxonomic diversity and phylogenetic relationships. These advances underscore the value of each newly discovered fossil for increasing our understanding of human evolutionary history. Although new areas in the Afar region, the Turkana Basin (Kenya), and other parts of Africa have been yielding important remains of early hominins (see Brown et al., 2013), Woranso-Mille, a site located in the north-central part of the Afar region of Ethiopia, has become one of the most prolific mid-Pliocene sources: in the last 15

* Corresponding author.
E-mail address: Yhaileselassie@asu.edu (Y. Haile-Selassie).

https://doi.org/10.1016/j.jhevol.2022.103265
0047-2484/

years, more than 200 hominin specimens of Pliocene age have been recovered from the site.

Woranso-Mille (Fig. 1) presents the strongest evidence for the contemporaneous presence of at least one non-*Au. afarensis* hominin species (e.g., *Au. deyiremeda* or a species represented by the Burtele foot) between 3.5 and 3.3 Ma (Haile-Selassie et al., 2012; Wood and Boyle, 2016), whereas the biological validity of other species named from the same period (*Au. deyiremeda*, *Au. bahrelghazali*, and *K. platyops*; Brunet et al., 1996; Leakey et al., 2001; Haile-Selassie et al., 2015) has been contested on various grounds (White, 2003; Kimbel et al., 2004; Wood and Boyle, 2016; but see Guy et al., 2008; Spoor et al., 2010; Haile-Selassie et al., 2016a). The Woranso-Mille fossils show that *Au. afarensis* and *Au. deyiremeda* coexisted in close geographic and temporal proximity at 3.5–3.3 Ma (Haile-Selassie et al., 2016a; Melillo et al., 2021). The 3.4 Ma Burtele partial foot from Woranso-Mille also indicated the presence of a bipedal locomotor adaptation different from that of the contemporaneous *Au. afarensis* (Haile-Selassie et al., 2012). Despite the close temporal and spatial provenience of the foot to specimens assigned to *Au. deyiremeda* (Haile-Selassie et al., 2015), it has not been assigned to any species yet, pending recovery of more complete craniodental specimens that are taxonomically informative and whose provenience could be clearly associated with the foot. Woranso-Mille fossiliferous sediments older than 3.5 Ma have yielded a 3.6-million-year-old partial skeleton and juvenile mandibles of *Au. afarensis* (Haile-Selassie et al., 2010a; Haile-Selassie and Ryan, 2019) and more recently a 3.8-million-year-old cranium of *Au. anamensis* (Haile-Selassie et al., 2019; Saylor et al., 2019). The *Au. anamensis* cranium (MRD-VP-1/1) not only expanded the previously known temporal range of the species (4.2–3.9 Ma; Leakey et al., 1995; Ward et al., 2001) but also provided a more complete understanding of the craniofacial anatomy of the species. Furthermore, it challenged the *Au. anamensis–Au. afarensis* anagenesis hypothesis by showing that the two species may have overlapped in time (Haile-Selassie et al., 2019).

The possible presence of *Au. anamensis* at Woranso-Mille was first hinted at by the two ca. 3.76 Ma partial mandibles (Haile-Selassie, 2010) that are described in detail here. Preliminary observations indicated that they retained a mosaic of dental and mandibular features intermediate between those of *Au. anamensis* and *Au. afarensis*. Given the presence of some features that are seen only in *Au. anamensis*, however, Haile-Selassie (2010) argued that these mandibles might be best assigned to *Au. anamensis*. Here, we provide a detailed comparative description of these specimens, particularly because more parts of one of the mandibles were recovered as a result of continued fieldwork, and newly assess their taxonomic affinity. This investigation will have significant implications for our understanding of the temporal and spatial distribution and dentognathic morphological variation in the earliest *Australopithecus* species in eastern Africa.

1.1. Discovery and preservation of MSD-VP-5/16 and MSD-VP-5/50

The left half of MSD-VP-5/16 was found in 2006 by Alemayehu Asfaw and the right half was found by a local Afar worker (Ali Kadir) in 2018, ca. 80 m south of the initial discovery (Figs. 2 and 3). The right half of the mandible joined the left half along the anterior corpus and symphyseal region. The corpus is well preserved with minimal to no distortion on its preserved parts on both sides. It does not have any sign of weathering or carnivore damage. Anteriorly, the adjoining break runs obliquely from the distal wall of the left I_2 at the alveolar margin to the base of the anterior corpus at the midline. The corpus on the left side is almost intact, extending posteriorly past the origin of the ramus, which is broken obliquely toward the gonial angle. Most of the ramus is missing on both sides except for the anteroinferior portion of the masseteric fossa at the M_3 level on the left side. The corpus base is partially preserved on both sides and in good condition, except for hairline cracks running along the length of the preserved corpus bases. Also on the lateral face of the left corpus base, there is another hairline crack that runs from the level of the C_1 posteriorly to the level of the mesial M_2. A small area of cortical bone (12.3 mm anteroposteriorly and 3.1 mm mediolaterally) is also flaked from the preserved distal terminus of the left corpus base at the M_2 level. The symphyseal region also shows some cracks that do not impact this region's morphology. A vertical crack runs down across the entire length of the median ridge formed by the incisal juga. Another crack, where the two halves joined, traverses obliquely from the base of the left I_2 to the midline at the base. On the right side, the corpus is broken vertically, but irregularly, posterior to the M_1. The preserved right lateral corpus shows a small triangular area of laterally deflected cortical bone close to the base at the P_4–M_1 level. There is also a faint crack running from the alveolar margin of the P_4 all the way to the base, traversing right through the mental foramen and extending to the corpus base. This crack continues to the medial side, running anterosuperiorly, and ends at the genioglossal fossa. The corpus base, as on the left side, has a hairline crack that traverses the entire length of the corpus base but causes no distortion. Also on the right side, the digastric fossa is depressed because of cortical bone loss at its center. The P_4 on the right side, the M_1s on both sides, and the left M_2 are preserved intact. A small piece of cortical bone is flaked from the distolingual corner of the left M_2 partially exposing its distal root. A small area of enamel is chipped from the apex of the left M_1 protoconid and a hairline crack runs across the occlusal surface of the hypoconid. The right M_1 protoconid was broken from the crown and its mesial half was recovered from a sieving operation. This molar also has a hairline crack that runs centrally from the central fovea to the distal marginal ridge. All of the anterior tooth crowns are missing, most of them broken at the level of the alveolar margin. The left M_3 crypt is partially preserved although its medial wall is broken. Its overall size and C_1 root length indicate that it probably belonged to a female individual while the unerupted M_3 with partially formed roots allows for an estimation of its developmental status (see section 3.1 for further details).

MSD-VP-5/50 is a left mandible preserving the P_3 to the M_3 found in 2009 by Woganu Amerga. It was found broken into numerous small pieces most of which joined (Figs. 4 and 5). The anterior corpus is partially preserved below the I_2 alveolus and at its base, the bone extends close to the midline. The anterior break is not fresh and the edges are rounded. Most of the inferior half of the ramus is preserved with some areas missing in the middle. The posteroinferior corner of the ramus above the gonial angle is also missing. The preserved corpus does not show substantial biotic or abiotic alterations and visible cracks are mostly from joined surfaces. The lateral and lingual alveolar margins are damaged to variable degrees. On the lateral side, the alveolar margin is unevenly chipped from C_1 to M_1 while it is preserved intact at both the distal M_2 and distal M_3 regions. On the lingual side, however, the margin is well preserved from P_4 to mesial M_2. Based on its overall corpus size, C_1 root robusticity, and length (judged from its preserved socket), it probably belonged to a male, while the amount of wear on its molars indicates that it was an older individual (Fig. 5).

1.2. Geological and paleoenvironmental context

Woranso-Mille (Fig. 1) is located in the central Afar region of Ethiopia north of Hadar where *Au. afarensis* is best known from 3.40 to 2.95 Ma (Kimbel et al., 2004; Campisano and Feibel, 2007, 2008; Kimbel and Delezene, 2009). Geological and paleontological work

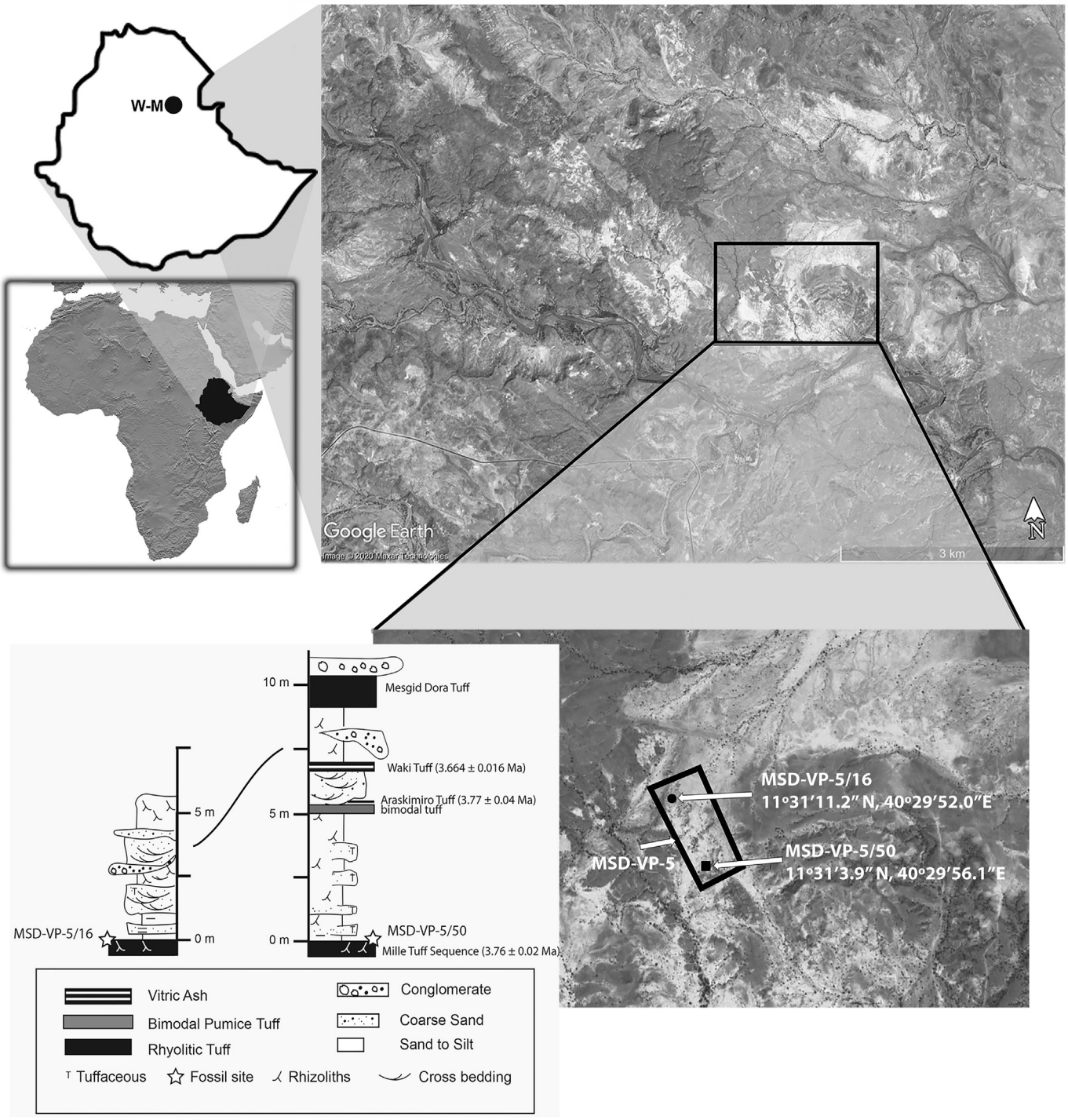

Figure 1. Location map and stratigraphy of the MSD-VP-5 locality. The stratigraphic section at the bottom left shows that MSD-VP-5/16 and MSD-VP-5/50 were recovered immediately above the Mille Tuff Sequence, dated to 3.76 Ma. The map of Africa on the left was taken from NASA and the images on the right were taken from Google Earth. W-M = Woranso-Mille.

at Woranso-Mille largely concentrated on the ca. 180-m-thick fossiliferous and sedimentary strata exposed in the modern Mille River catchment. These strata are radiometrically dated to 3.8–3.2 Ma, with the faunal assemblages divided into five age groups based on dated marker tuffs and paleomagnetic boundaries (3.8–3.66, 3.66–3.57, 3.57–3.47, 3.47–3.33, and 3.33–3.2 Ma). Mesgid Dora locality 5 (MSD-VP-5), one of nine localities in the MSD collection area, is among the older localities in the 3.8–3.66 Ma time interval (Fig. 1). The general stratigraphy of locality MSD-VP-5 has been described previously, including $^{40}Ar/^{39}Ar$ dating and tephrochemical correlation of volcanic tuffs and mapping of volcanic tuffs and channel sandstone bodies (Deino et al., 2010; Saylor et al., 2016). The fossil specimens described here were collected ~250 m apart, from the top surface of a felsic

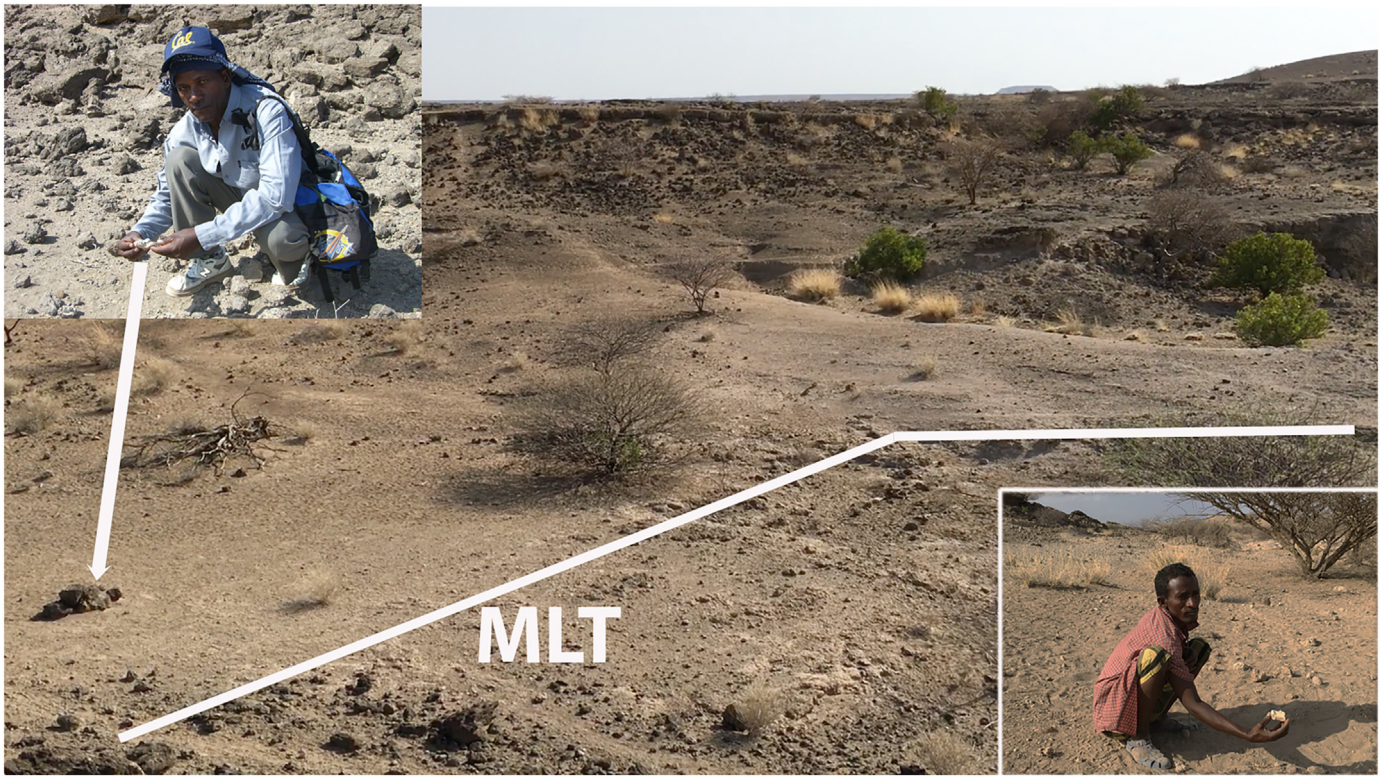

Figure 2. Discovery location of MSD-VP-5/16. The white lines show the extensive Mille Tuff Sequence (3.76 Ma) immediately below the fossil discovery. Inset top left: Alemayehu Asfaw discovered the left half of the mandible in February 2006. Inset bottom right: Ali Kadir found the right half in February 2018, ca. 80 m south of where the left half was found.

lapillistone tuff that is part of the Mille Tuff sequence (Fig. 1). In most locations the tuffs in the Mille sequence are airfall deposits (Saylor et al., 2016, 2019), but some have been fluvially reworked into ~5 m of interbedded and cross-bedded tuffaceous sandstone, siltstone and discontinuous tuff that lie between the fossil collection horizon and an overlying bimodal tuff composed of basaltic and felsic pumice (Fig. 1). Ages for the Mille Tuff sequence (3.76 ± 0.02 Ma) and the Araskimiro Tuff (3.77 ± 0.04 Ma), a felsic pumice tuff above the bimodal tuff, are statistically indistinguishable (Deino et al., 2010; Saylor et al., 2016).

The sequence of rhyolitic and basaltic lapillistone tuffs and tuffaceous sedimentary rocks that contains the fossil collection horizon is overlain by coarse channelized sandstone followed by the Waki Tuff (3.664 ± 0.016 Ma), an extrabasinal vitric ash that has chronological and geochemical characteristics compatible with the Lomogol Tuff in the Omo-Turkana Basin (Saylor et al., 2016). The pumice tuffs, sandstone, and the Waki Tuff have been traced from the MSD-VP-5/50 discovery location to within 50 m of the MSD-VP-5/16 discovery (Saylor et al., 2016), though in the near proximity to the site itself these beds are missing because of subsequent incision by an intraformational fluvial channel (Fig. 6). Conglomeratic channel sandstones contain diverse basaltic and rhyolitic clasts up to 5 cm across and form northwest-southeast to northeast-southwest oriented curvilinear bodies that are 20–30 m across and on the order of several hundred meters in length. These channel sandstones were deposited in a broad paleo-valley that is ~600 m across and oriented northwest-southeast. The Mesgid Dora Tuff, which lies stratigraphically above the Waki Tuff, drapes more than 15 m of relief along this paleo-valley and varies from airfall deposits that are as much as ~10 m above the Waki Tuff to fluvially reworked channel deposits directly overlying the Mille Tuff Sequence (Saylor et al., 2016). Beds of limestone and platy mudstones formed in shallow water bodies within the paleo-valley. Lack of well-developed paleosols is consistent with a quickly aggrading depositional system and short-lived land surfaces. The maximum age of MSD-VP-5/16 and MSD-VP-5/50 is established by the Mille Tuff Sequence (3.76 ± 0.02 Ma), and the minimum age by the Waki Tuff (3.664 ± 0.016 Ma), though the specimens are more likely closer to the maximum age because they were recovered from immediately above the Mille Tuff Sequence (Fig. 1).

The faunal assemblage from MSD-VP-5 is similar to that from contemporaneous and slightly younger Woranso-Mille localities at Aralee Issie (Haile-Selassie et al., 2010b). Previous multiproxy paleoecological studies of the faunal assemblage at MSD (3.76–3.57 Ma) indicated heterogeneous habitats with dense vegetation along a paleo-river grading into more open habitats away from the riparian zone (Curran and Haile-Selassie, 2016). Su and Haile-Selassie (2022) further showed that the nonhominin faunal community structure at MSDC (a fossil collection area that includes MSD-VP-5 and two other nearby localities dated to between 3.76 and 3.66 Ma) indicates heterogeneous habitats while it appears that woodland habitats were predominant.

2. Materials and methods

Mandibles are relatively well represented in the hominin fossil record and characters of corpus morphology have played a significant role in species recognition and phylogenetic analyses (Johanson et al., 1978; Johanson and White, 1979; White and Johanson, 1982; Chamberlain and Wood, 1985; Leakey et al., 1995, 1998; Brunet et al., 1996; Strait et al., 1997; Ward et al., 2001; Strait and Grine, 2004; Kimbel et al., 2004, 2006; Alemseged et al., 2005; Guy et al., 2008; Haile-Selassie et al., 2015). However, mandibular sample size is highly variable across hominin taxa. For example,

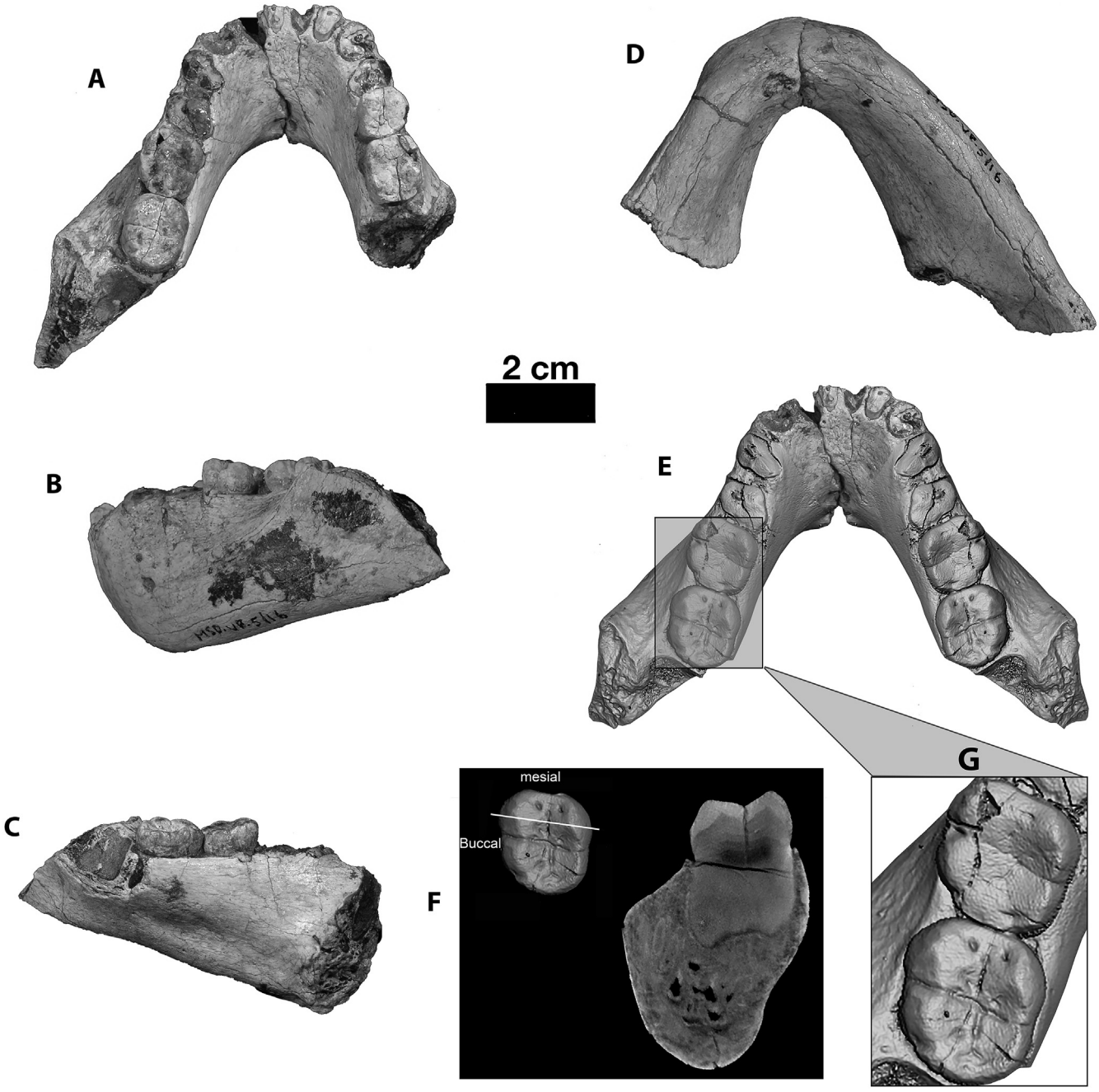

Figure 3. MSD-VP-5/16. A) occlusal view; B) left lateral view; C) left slightly oblique medial view; D) basal view; E) dental arcade shape reconstructed by mirror-imaging the left side; F) posterior view of a coronal section at left M_2. The white line in the inset M_2 shows the plane of section through the protoconid and metaconid cusp apices; G) occlusal view of the left M_{1-2}.

there are only a few mandibles of *Ardipithecus ramidus* recovered from Aramis and Gona (Semaw et al., 2005; White et al., 2009), whereas there are more than 60 known mandibles of *Au. afarensis*, mostly from Hadar (Ethiopia), sampling from juvenile to adult individuals (White, 1977; White and Johanson, 1982; Kimbel et al., 2004, 2006; Kimbel and Delezene, 2009; Harrison, 2011; Glowacka et al., 2017). The mandibular sample of *Au. anamensis*, including small corpus fragments, is limited to 11 specimens from Kanapoi and Allia Bay (Leakey et al., 1995; Ward et al., 2001, 2020), and there are only two known mandibles of *Au. deyiremeda* (Haile-Selassie et al., 2015).

All morphological descriptions of MSD-VP-5/16 and MSD-VP-5/50 reported here are based on observations of the original specimens, which are housed in the National Museum of Ethiopia, Addis Ababa. In addition, microcomputed tomography (μCT) scans were used for some parts of the description. MSD-VP-5/50 and the left half of MSD-VP-5/16 were scanned using a GE v|tome|x L300 industrial multiscale microcomputed tomography scanner at the Pennsylvania State University Center for Quantitative Imaging. Unfortunately, MSD-VP-5/16 was not μCT rescanned after the discovery of the right half in 2018. The left half of MSD-VP-5/16 was scanned on an XTEK microfocus x-ray tube with source energy

Figure 4. MSD-VP-5/50 before restoration. It was discovered in two major pieces of the corpus with the P_4–M_2 and the M_3 in place. The P_3 and all of the pieces of the ramus ($n = 32$) were found by sieving.

settings of 180 kV and 0.250 μA, and voxel size of 0.042 mm (x, y) and 0.0455 mm (z). MSD-VP-5/50 was scanned using a high-energy Pantak x-ray tube with source energy settings of 250 kV and 2.0 μA, and voxel size of 0.076 mm (x, y) and 0.074 mm (z). Analysis of μCT scan data and processing was performed using Avizo v. 9.5.0 (Thermo Fisher Scientific, Waltham).

The comparative sample includes all published dentally adult mandibles and associated teeth of *Ar. ramidus* ($n = 3$) from Middle Awash and Gona (Ethiopia), *Au. anamensis* ($n = 11$) from Kanapoi and Allia Bay (Kenya), *Au. afarensis* ($n = 41$) from Hadar and Maka (Ethiopia) and Laetoli (Tanzania), and *Au. deyiremeda* ($n = 2$) from Woranso-Mille (Table 1). Morphological observations on *Ar. ramidus*, Hadar and Maka *Au. afarensis*, and *Au. deyiremeda* mandibles were made on the originals housed at the National Museum of Ethiopia. The originals of *Au. anamensis* were studied at the National Museums of Kenya in Nairobi and supplemented by published descriptions (Ward et al., 2001, 2013, 2020). The Laetoli *Au. afarensis* material was analyzed based on published descriptions (White, 1977, 1980; Harrison, 2011), with additional observations made on casts housed at the Cleveland Museum of Natural History. Mandibular and dental terminology used in the description follows White (1977, 1980) and White and Johanson (1982).

The comparative assessment of the Woranso-Mille mandibles is based on qualitative description of mandibular morphology (corpus, symphysis, ramus) and dentition as well as quantitative analysis of the corpus and dentition. Mandibular and dental measurements of the Woranso-Mille specimens were taken on the original specimens using digital calipers with accuracy to the nearest 0.02 mm. Descriptive statistics for mandibular and dental measurements of the comparative sample (Tables 2 and 3) were compiled from published sources (White, 1977, 1980; White et al., 2000; Ward et al., 2001, 2013, 2020; Kimbel et al., 2004; Suwa et al., 2009a). We conducted comparative analyses using dental and mandibular metric measurements. The mesiodistal (MD) and buccolingual (BL) dimensions of the teeth preserved in the two mandibles described here were compared to those of the comparative species (Table 1). We calculated the square root of crown area ($\sqrt{MD \times BL}$) for each tooth preserved in the two Woranso-Mille mandibles and the comparative samples. We generated box-and-whisker plots to examine the range of variation in the crown area of each tooth (P_3–M_3) preserved in the mandibles of *Ar. ramidus* (P_3

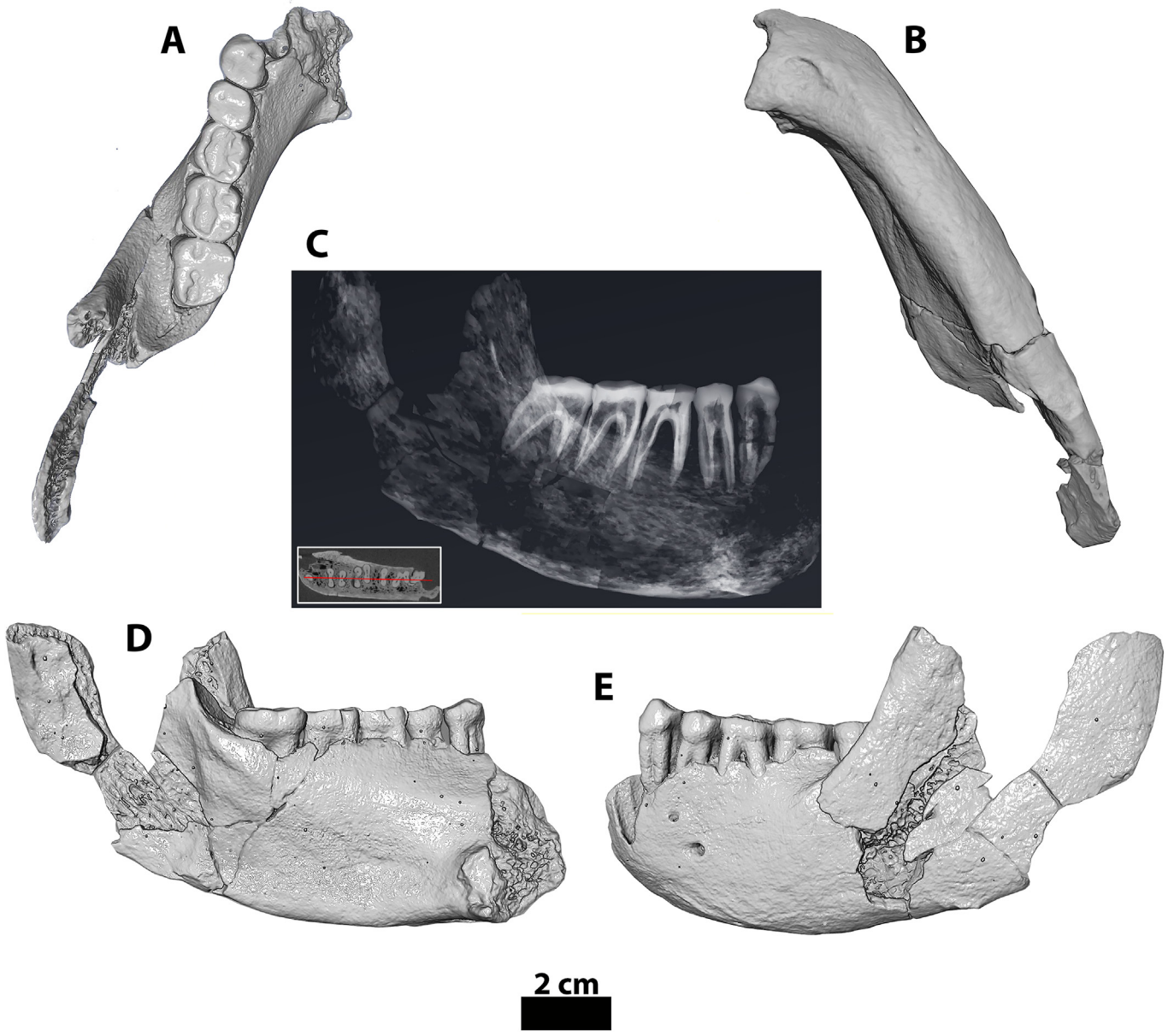

Figure 5. MSD-VP-5/50. A) occlusal view; B) basal view; C) orientation and radicular morphology of the roots in the preserved teeth (P_3–M_3). The red line in the inset on the bottom left refers to the sagittal plane of section; D) medial view; E) lateral view. All figures were generated from μCT scan images using Avizo v. 9.5.0 (Thermo Fisher Scientific, Waltham). (For interpretation of the references to color in this figure legend, the reader is referred to the Web version of this article).

not included), *Au. anamensis*, *Au. afarensis*, and *Au. deyiremeda*. For crown area comparisons, we included only those that have the entire P_3–M_3 preserved. This allows us particularly to evaluate if on average the P_3 is larger than the P_4 or the M_2 is larger than the M_3, or vice versa.

We conducted correlation analysis to investigate whether there is a significant association between two quantitative variables of the corpus (height and breadth at the M_1 level). Corpus height was measured as the vertical distance from the alveolar margin to the corpus base at the mid-M_1 level and corpus breadth was measured as the mediolateral thickness of the corpus at the mid-M_1 level perpendicular to the height. We first constructed a scatter diagram for *Au. afarensis* ($n = 24$) using the two variables and generated Pearson's correlation coefficient (r) and calculated the *p*-value. We generated a 95% confidence interval (CI) ellipse for the *Au. afarensis* sample using R v. 4.2.1 to see how many of the specimens fall within the interval. We also used the *Au. afarensis* 95% CI to evaluate whether mandibular shape of the Woranso-Mille and *Au. deyiremeda* mandibles falls within or outside this interval. For this, we constructed three additional scatter diagrams adding to the *Au. afarensis* sample: 1) *Au. anamensis* ($n = 3$); 2) the Woranso-Mille mandibles ($n = 2$); and 3) *Au. deyiremeda* ($n = 2$) and Woranso-Mille mandibles all together. Pearson's correlation coefficient and *p*-values were generated for all three scatter diagrams. This allowed us to examine how the inclusion and/or exclusion of the Woranso-Mille mandibles, or the inclusion of *Au. deyiremeda* to the *Au.*

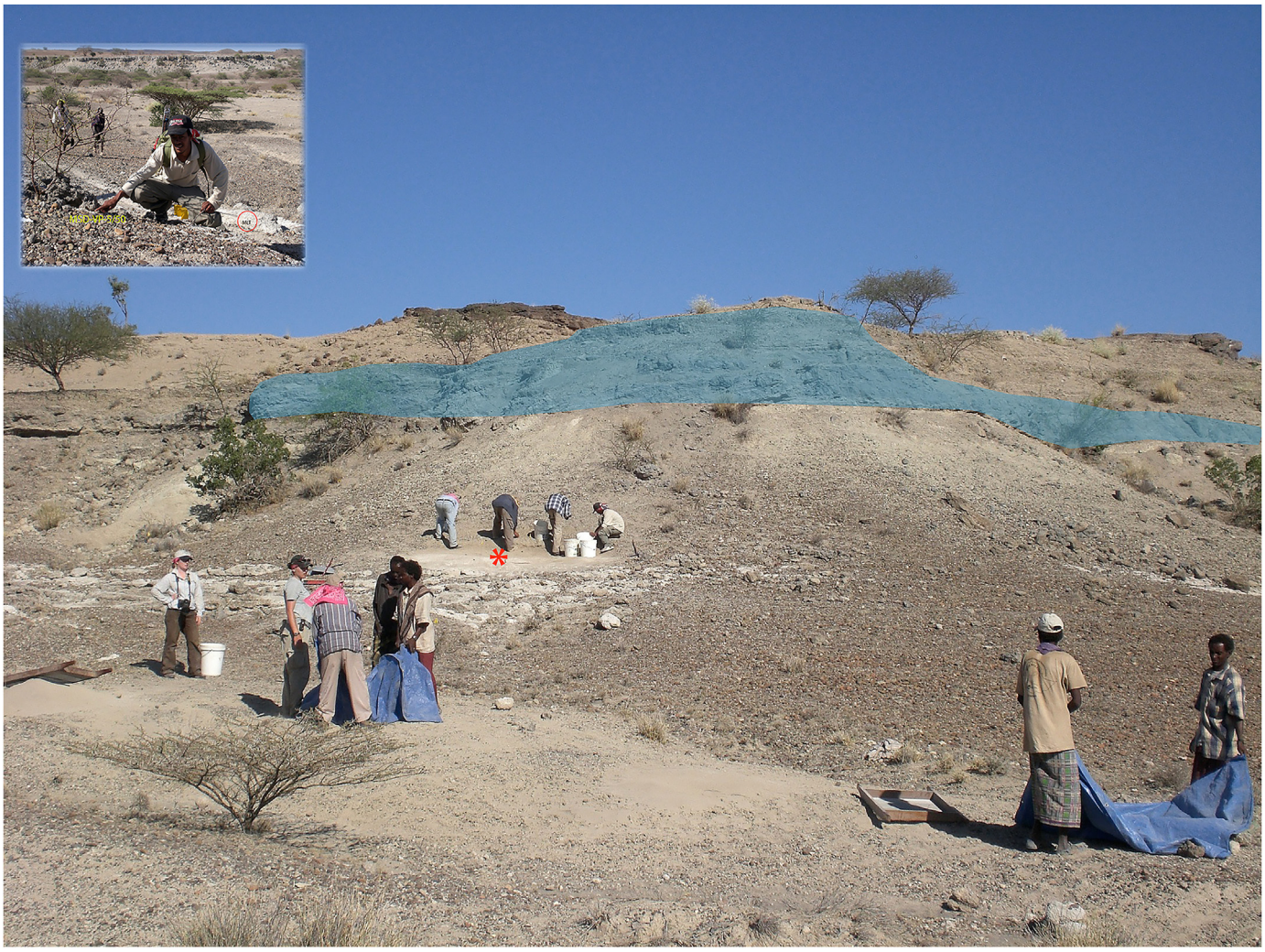

Figure 6. Discovery location of MSD-VP-5/50 (red star) above the Mille Tuff Sequence. The coarse channelized sandstone (shown in blue gray) cuts through the Araskimiro Tuff and the Basalt Rhyolitic Tuff and is overlain by the Waki Tuff (3.66 Ma), providing a minimum age for the specimen. Woganu Amerga (inset on the upper left corner) discovered the first piece of the specimen in 2009.

anamensis and *Au. afarensis* sample impacts the r and *p*-values. Box-and-whisker and scatter plots were generated using Microsoft Excel for Mac v. 16.61.1 (Microsoft, Redmond).

3. Results

3.1. Developmental age of MSD-VP-5/16

MSD-VP-5/16 is a mandible preserving the left M_1–M_2 and right P_4–M_1 (Fig. 3). The first and second molars display moderate to slight wear. If the MSD-VP-5/16 individual is not a dental adult, its developmental age is extremely close to that of an adult, as the left M_3 crown is judged to have been in the process of emerging (likely beyond gingival emergence) or to be near reaching the level of functional occlusion. This assessment is based primarily on the state of development of the M_3 alveolar socket, the state of root apical closure of the M_2, and the length and developmental status of the canine root (Fig. 7).

The mesial wall of the M_3 alveolar socket measures 8.1 mm; this is likely a slight underestimate of its true length, given that the alveolar margin in the interproximal region is slightly broken/eroded, missing at most the superior ~1 mm (see white arrow in Fig. 7B). In describing DNH 12, a right mandibular fragment that preserves part of the crown of an erupting M_3, Moggi-Cecchi et al. (2010) noted that this tooth preserves ~8 mm of its mesial root, supporting the notion that the M_3 roots of MSD-VP-5/16 are developed enough to support a molar that is emerging, at the very least. The inferiormost portion of the distal alveolar socket of the M_3 is also present, as is the interradicular septum separating the two alveoli (Fig. 7C). The superiormost tip of this septum (left arrow in Fig. 7C) looks to be slightly damaged, given that this region has filled-in with matrix, and sits slightly (ca. 2 mm) inferior to the level of the M_1 and M_2 interradicular septa. The presence of a clear septum indicates substantial root development of both the mesial and distal M_3 root plates. Based on the length of the preserved root socket, we judge the state of M_3 root development to be at least at the stage $R_{½}$ and thus similar to that of A.L. 486-1 (Dean et al., 2020). In addition, the mesial wall of the M_3 root alveolar socket in MSD-VP-5/16 shows no sign of a cervical impression, which would be present if the crown were situated inferior to the alveolar margin, and suggests that it is the mesial margin of the M_3 root plate that sits adjacent to the mesial alveolar margin for its entire length.

Table 1
List of the study specimens from Woranso-Mille and Pliocene hominin mandibles used in the comparative analysis.

Species	Specimen number	Element	Recovery site	References
	MSD-VP-5/16	Mandible with dentition (left M_{1-2}, right P_4–M_1, left I_1, C_1–P_4 roots, I_2–P_3 roots)	Woranso-Mille	Haile-Selassie, 2010; this study
	MSD-VP-5/50	Left mandible with dentition (P_3–M_3)	Woranso-Mille	Haile-Selassie, 2010; this study
Ar. ramidus				
	ARA-VP-6/500	Left mandible fragment (C_1–M_3)	Middle Awash, Ethiopia	Suwa et al., 2009b
	ARA-VP-1/401	Mandible with dentition	Middle Awash, Ethiopia	Suwa et al., 2009b
	GWM3/P1	Right mandible corpus fragment	Gona	Semaw et al., 2005
Au. anamensis				
	KNM-ER 20432	Left mandible fragment with P_{3-4}	Allia Bay, Kenya	Leakey et al., 1995; Ward et al., 2001
	KNM-KP 29281	Mandible with dentition (left and right I_1-M_3)	Kanapoi, Kenya	Leakey et al., 1995; Ward et al., 2001
	KNM-KP 29286	Mandible fragments and associated dentition (right I_1, left and right I_2–M_3)	Kanapoi, Kenya	Leakey et al., 1995; Ward et al., 2001
	KNM-KP 29287	Right and left mandible fragments with molar roots	Kanapoi, Kenya	Leakey et al., 1995; Ward et al., 2001
	KNM-KP 30500	Left and right mandible fragments with dentition (left P_3, M_{1-3}; right P_4–M_3)	Kanapoi, Kenya	Ward et al., 2001
	KNM-KP 31712	Associated juvenile mandible and dental fragments	Kanapoi, Kenya	Ward et al., 2001
	KNM-KP 31713	Right mandible with tooth fragments	Kanapoi, Kenya	Ward et al., 2001
	KNM-KP 31718	Right mandible fragment (M_{2-3})	Kanapoi, Kenya	Ward et al., 2001
	KNM-KP 47956	Left edentulous partial mandible (M_{2-3} and part of M_1 roots)	Kanapoi, Kenya	Ward et al., 2013
	KNM-KP 53160	Mandible with left M_2–right M_2	Kanapoi, Kenya	Ward et al., 2020
	KNM-KP 59499	Mandibular corpus fragment	Kanapoi, Kenya	Ward et al., 2020
Au. afarensis				
	A.L. 128-23	Right mandible fragment (C_1–M_2)	Hadar, Ethiopia	Johanson et al., 1982
	A.L. 145-35	Left mandible fragment (P_3–M_2)	Hadar, Ethiopia	Johanson et al., 1982
	A.L. 188-1	Right mandible fragment (M_{2-3})	Hadar, Ethiopia	Johanson et al., 1982
	A.L. 198-1	Left mandible fragment (C_1–M_3)	Hadar, Ethiopia	Johanson et al., 1982
	A.L. 198-22	Left mandible fragment (M_1, M_2 fragment)	Hadar, Ethiopia	Kimbel et al., 2004
	A.L. 207-13	Left mandible fragment (P_3–M_2)	Hadar, Ethiopia	Johanson et al., 1982
	A.L. 225-8	Left mandible fragment (M_{1-3})	Hadar, Ethiopia	Kimbel et al., 2004
	A.L. 228-2	Left mandible fragment (M_1), P_4	Hadar, Ethiopia	Kimbel et al., 2004
	A.L. 266-1	Mandible (left P_3–M_1, right P_3–M_3)	Hadar, Ethiopia	Johanson et al., 1982
	A.L. 277-1	Left mandible fragment (C_1–M_2)	Hadar, Ethiopia	Johanson et al., 1982
	A.L. 311-1	Left mandible fragment (P_3)	Hadar, Ethiopia	Johanson et al., 1982
	A.L. 315-22	Right mandible fragment (P_3, M_1)	Hadar, Ethiopia	Kimbel et al., 2004
	A.L. 330-5	Mandible (left C_1 fragment; right P_4–M_3)	Hadar, Ethiopia	Kimbel et al., 2004
	A.L. 330-7	Right mandible fragment (P_4, M_1)	Hadar, Ethiopia	Kimbel et al., 2004
	A.L. 333w-1	Left and right mandible fragments (left P_3–M_2; right P_4–M_2)	Hadar, Ethiopia	Johanson et al., 1982
	A.L. 333w-12	Right mandible fragment (M_1)	Hadar, Ethiopia	Johanson et al., 1982
	A.L. 333w-27	Left mandible fragment (M_2)	Hadar, Ethiopia	Johanson et al., 1982
	A.L. 333w-46	Right mandible fragment (P_3)	Hadar, Ethiopia	Johanson et al., 1982
	A.L. 333w-57	Left mandible fragment (M_{2-3})	Hadar, Ethiopia	Johanson et al., 1982
	A.L. 333w-59	Left mandible fragment (M_{2-3})	Hadar, Ethiopia	Johanson et al., 1982
	A.L. 333w-60/32	Mandible fragments (left P_3–M_3; right I_1–C_1)	Hadar, Ethiopia	Johanson et al., 1982; Kimbel and Delezene, 2009
	A.L. 333-59	Right mandible fragment (M_{2-3})	Hadar, Ethiopia	Johanson et al., 1982
	A.L. 333-74	Left mandible fragment (M_{1-3})	Hadar, Ethiopia	Johanson et al., 1982
	A.L. 400-1a	Mandible (left I_1–M_3; right I_2–M_3)	Hadar, Ethiopia	Johanson et al., 1982
	A.L. 411-1	Right mandible fragment (M_{1-3})	Hadar, Ethiopia	Johanson et al., 1982
	A.L. 417-1	Left and right mandible fragments (left C_1–M_3; right M_{2-3})	Hadar, Ethiopia	Kimbel et al., 2004
	A.L. 418-1	Left mandible fragment (M_2)	Hadar, Ethiopia	Kimbel et al., 2004
	A.L. 432-1	Right mandible fragment (M_{2-3} fragments)	Hadar, Ethiopia	Kimbel et al., 2004
	A.L. 433-1a–b	a) Right mandible fragment (P_4 fragment); b) left mandible fragment	Hadar, Ethiopia	Kimbel et al., 2004
	A.L. 437-1	Left mandible fragment (P_4–M_3)	Hadar, Ethiopia	Kimbel et al., 2004
	A.L. 437-2a	Mandible (left I_1–C fragments; right I_1–I_2 fragments; right M_{2-3} fragments)	Hadar, Ethiopia	Kimbel et al., 2004
	A.L. 440-1	Right mandible fragment (C_1, P_3; left I_1, C_1, P_4–M_2)	Hadar, Ethiopia	Kimbel et al., 2004
	A.L. 443-1	Left mandible fragment (P_4, M_2)	Hadar, Ethiopia	Kimbel et al., 2004
	A.L. 582-1	Mandible (I_1, left P_4–M_1; right P_3–M_1 fragments)	Hadar, Ethiopia	Kimbel et al., 2004
	A.L. 620-1	Left mandible fragment (M_3)	Hadar, Ethiopia	Kimbel et al., 2004
	A.L. 996-1	Left mandible fragment (P_4–M_1)	Hadar, Ethiopia	Kimbel et al., 2004
	DIK 2-1	Left mandible fragment (P_3, M_1; isolated M_2 fragment, M_3)	Dikika, Ethiopia	Alemseged et al., 2005
	MAK-VP-1/2	Right mandible fragment (M_{1-3})	Middle Awash, Ethiopia	White et al., 2000
	MAK-VP-1/12	Mandible (left I_2–M_3; right P_3–M_3)	Middle Awash, Ethiopia	White et al., 2000
	NFR-VP-1/29	Mandible (left I_2, P_4–M_3; right P_4–M_3)	Woranso-Mille, Ethiopia	Haile-Selassie et al., 2016b
	L.H. 4	Mandible (right C_1 fragment–M_3; left M_{1-3})	Laetoli, Tanzania	White, 1977
Au. deyiremeda				
	BRT-VP-3/14	(Apical halves of left I_2–right I_2, right P_3–M_3)	Woranso-Mille, Ethiopia	Haile-Selassie et al., 2015
	WYT-VP-2/10	Edentulous mandible	Woranso-Mille, Ethiopia	Haile-Selassie et al., 2015

Table 2
Dental measurements of Woranso-Mille specimens and dental summary statistics of the comparative species. The comparative data were compiled from Leakey et al. (1995), Ward et al. (2001), Kimbel et al. (2004), Haile-Selassie et al. (2010a, 2015), and White et al. (2015). All measurements are provided in mm.[a]

	Mesiodistal					Buccolingual				
	n	Mean	SD	Min	Max	*n*	Mean	SD	Min	Max
P_3										
MSD-VP-5/50	–	10.4	–	–	–	–	10.1	–	–	–
Ar. ramidus	–	–	–	–	–	–	–	–	–	–
Au. anamensis	9	9.7	0.62	8.7	10.5	6	11.4	1.2	9.9	13.6
Au. afarensis	30	9.6	1.08	7.9	12.6	30	10.4	1.11	8.2	13.8
Au. deyiremeda	1	7.6	–	–	–	–	10.8	–	–	–
P_4										
MSD-VP-5/16	–	9.5	–	–	–	–	9.9	–	–	–
MSD-VP-5/50	–	9.1	–	–	–	–	10.3	–	–	–
Ar. ramidus	8	8	0.65	7.3	8.9	8	9.4	0.47	8.7	10.2
Au. anamensis	10	9.3	0.91	7.3	10.1	10	11.1	1.31	9.5	13.2
Au. afarensis	26	9.8	1.04	7.7	11.4	23	11.1	0.91	9.2	12.8
Au. deyiremeda	1	8.2	–	–	–	1	10.6	–	–	–
M_1										
MSD-VP-5/16	–	12.5[b]	–	–	–	–	11.9[c]	–	–	–
MSD-VP-5/50	–	11.6	–	–	–	–	11.7	–	–	–
Ar. ramidus	11	11.3	0.64	10.2	12.5	10	10.5	0.47	9.9	11.5
Au. anamensis	12	12.5	0.86	11.6	13.8	13	11.8	0.84	10.4	13.5
Au. afarensis	34	13.2	0.91	11.2	15.6	29	12.5	0.88	10.9	14
Au. deyiremeda	1	(12.6)	–	–	–	1	(12.6)	–	–	–
M_2										
MSD-VP-5/16	–	13.7	–	–	–	–	12.3	–	–	–
MSD-VP-5/50	–	13.8	–	–	–	–	13.2	–	–	–
Ar. ramidus	8	13	0.61	12.4	14.1	8	11.9	0.4	11.3	12.5
Au. anamensis	10	14.7	0.92	13.8	16.1	10	13.2	0.99	12	14.9
Au. afarensis	36	14.3	1.26	11.5	16.5	32	13.3	1.07	10.9	15.2
Au. deyiremeda	1	(14.8)	–	–	–	1	(13.8)	–	–	–
M_3										
MSD-VP-5/50	–	16.2	–	–	–	–	13.9	–	–	–
Ar. ramidus	7	12.5	0.72	11.3	13.2	8	11.8	0.91	10.4	13.1
Au. anamensis	10	15.3	1.3	13.6	17.2	9	13.6	0.99	12.1	15.2
Au. afarensis	27	15.3	1.29	13.4	18.1	24	13.5	0.99	11.3	15.3
Au. deyiremeda	1	(15.8)	–	–	–	1	(13.4)	–	–	–

[a] Measurements in parentheses are corrected for interproximal wear and/or taphonomic alterations.
[b] Average of left and right sides.
[c] Left side only.

Table 3
Corpus dimensions in the Woranso-Mille mandibles and statistical summary of comparative species. Summary statistics compiled from White et al. (2000), Kimbel et al. (2004), Haile-Selassie et al. (2015), and Melillo et al. (2021).

	Corpus height at M_1					Corpus breadth at M_1					Breadth/height ratio				
	n	Mean	Sd	Min	Max	*n*	Mean	Sd	Min	Max	*n*	Mean	Sd	Min	Max
MSD-VP-5/16	–	30.8	–	–	–	–	20.0	–	–	–	–	64.9	–	–	–
MSD-VP-5/50	–	44.6	–	–	–	–	21.2	–	–	–	–	47.5	–	–	–
Au. anamensis	5	34.0	6.6	26	40.5	3	18.8	1.0	18.0	20.0	3	55.3	6.4	49.4	62.1
Au. afarensis	25	33.9	4.1	27.8	41.3	28	19.8	2.2	15.8	24.7	24	58.6	6.6	48.4	75.9
Au. deyiremeda	2	33.9		33.4[a]	34.3	2	25.2		24.1[a]	26.2	2	74.3		72.2	76.4

[a] Values are averaged from left and right sides.

The mesial and distal roots of the M_2 of MSD-VP-5/16 are well developed and preserve only very slightly open apices, indicating that they are at the apex partially closed (i.e., $A_{½}$) stage of development (Fig. 8). From the μCT images, it is clear that the depth of the mesial M_3 root socket extends approximately two-thirds of the way down the length of the distal M_2 root, indicating the advanced developmental state of the former's root relative to that of the latter.

The left C_1 root is ~19 mm long (Fig. 9A–C) and extends inferiorly beyond the level of the mental foramen (see Fig. 3D). Given its length, it is reasonable to assume that most, if not all, of adult canine root length has been achieved. The apex of the root, however, is still open and is judged to be between the root complete (R_c) and apex partially-closed ($A_{½}$) stage of development.

3.2. Corpus morphology of MSD-VP-5/16

Occlusal aspect The preserved incisor and C_1 region of the corpus indicates that these teeth formed a tight arc and the transition from anterior to lateral corpus is at the C_1. The transition is abrupt due to a well-developed C_1 jugum and weak P_3 jugum. This makes the arcade more U-shaped anteriorly while the postcanine teeth moderately diverge posteriorly. The preserved C_1 roots and postcanine teeth indicate that the C_1s were aligned with the long axis of the postcanine tooth row, as indicated by μCT scan images of the specimen (Fig. 10B). The posteriormost point of the symphysis, which appears to be on the inferior transverse torus, is at the mesial edge of the P_4.

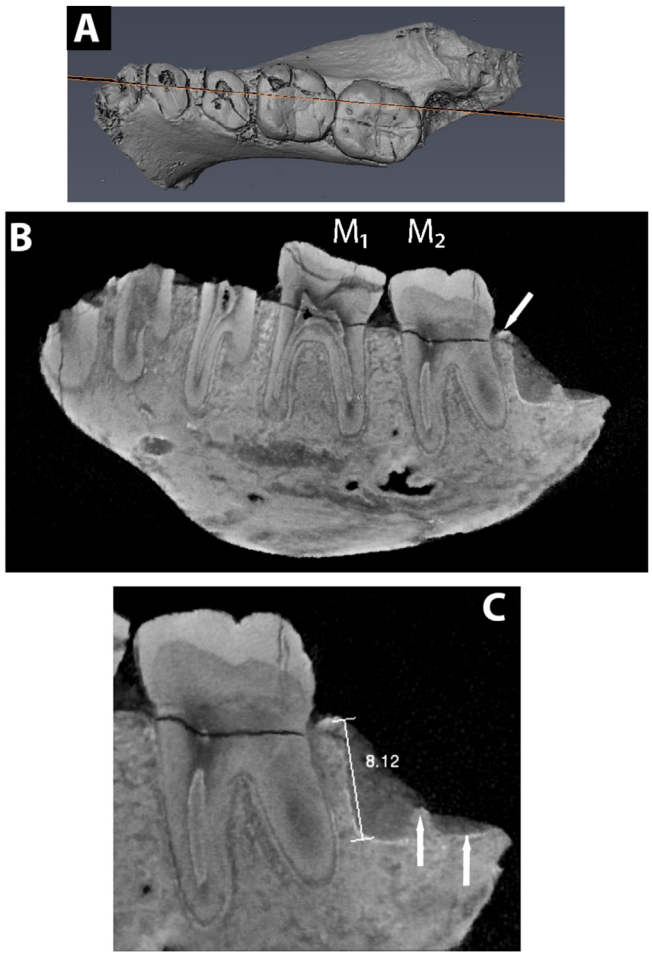

Figure 7. MSD-VP-5/16 molar roots. A) surface model from μCT scan showing plane of section used to generate individual slice through M_3 crypt; B) section showing M_3 crypt development and the lack of cervical impression on the interdental septum (white arrow); C) measurement of alveolar depth (in mm) of the mesial root plate. White arrows show the presence of an interradicular septum (left arrow) and the inferiormost extent of the distal root of the M_3 (right arrow).

Anterior aspect The alveolar margin is intact only below the right I_2 where it is sharp and steeply sweeps inferiorly to the C_1. The combined jugum of the central and lateral incisors forms a slightly raised triangular midline prominence that runs inferiorly for two-thirds of the superoinferior length of the symphysis before merging with the basal margin of the anterior corpus. Lateral to the I_2 jugum is a shallow vertical depression posterolaterally bounded by the strong C_1 jugum. This hollow extends inferiorly to the level of the C_1 root tip.

Posterior aspect The lingual alveolar margin of the anterior teeth is broken for the most part, except at right I_2 and C_1 where it is sharp and U-shaped. The postincisive plane is steep and strongly hollowed transversely, but almost flat vertically. It gently sweeps posteroinferiorly to terminate in a weakly developed superior transverse torus. At the center of its inferior edge is a centrally positioned shallow and roughly circular genioglossal fossa. Minor bone flakes in this region prohibit detailed description of its anatomy. The inferior transverse torus is also weakly developed and its posteriormost extension is only slightly more posterior than that of the superior transverse torus. Although some breakage is apparent, clearly visible rugosities close to the base of the inferior transverse torus at the midline indicate that the mental spines were strongly developed.

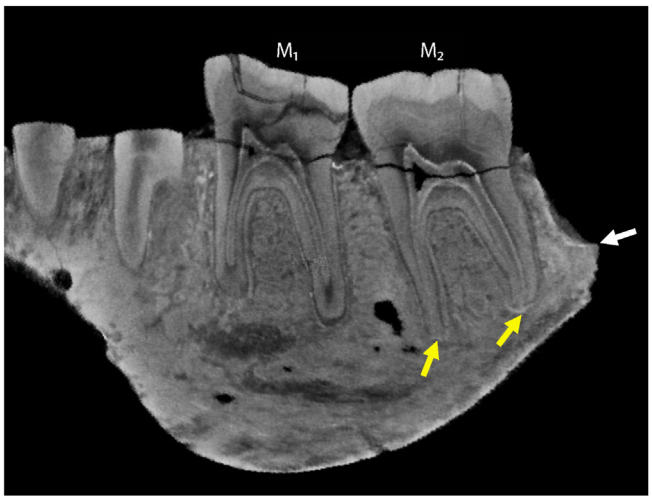

Figure 8. Mesial and distal M_2 root development illustrating the partial closure of the apices in both root plates (yellow arrows). Note the position of the inferiormost extent of the M_3 socket (white arrow) extending approximately two-thirds of the length of the M_2 distal root. The section in this figure is taken in a slightly different plane than the section in Fig. 7, to focus on the roots of the M_2. (For interpretation of the references to color in this figure legend, the reader is referred to the Web version of this article).

Lateral aspect Description of the lateral aspect is based largely on the left side (Fig. 3B) with some additional observations on the right side. In lateral view, the superior half of the anterior margin of the symphysis is nearly vertical and barely sloping. The inferior half of the symphysis sweeps abruptly posteroinferiorly. Corpus height substantially decreases from C_1 (31.3 mm) to M_2 (24.7 mm). Perpendicular to the alveolar margin, the symphysis is 33.7 mm superoinferiorly and 19.5 mm anteroposteriorly. The latter is estimated from a μCT-based cross-section of the symphysis preserved on the left side as the horizontal distance between two vertical lines drawn at anteriormost and posteriormost points of the symphysis perpendicular to the alveolar margin. The alveolar margin at the M_{1-2} level is sharp and straight. Anteriorly, the alveolar margin is mostly abraded or chipped and the cortical bone on the anterior face of the left I_2 root is missing and exposes the root socket. The preserved molar row on the left side shows a weak Curve of Spee. The strong C_1 jugum bulges laterally, fading inferiorly below the mental foramen. The C_1 jugum merges with a faintly palpable P_3 jugum to anteriorly bound a shallow depression below the premolars. Posteriorly, this depression is demarcated by a mild jugum formed by the mesial root of the M_1. Inferiorly, it terminates at the level of the mental foramen at the anteriormost terminus of the oblique line. The mental foramen on the left side is circular with a diameter of 3.1 mm (right side is an anteroposteriorly elongated oval; 3.6 mm anteroposteriorly and 2.0 mm superoinferiorly) situated at mesial P_3 position, at mid-corpus height, with its center 15.7 mm above the base and 15.1 mm below the preserved alveolar margin. The mental foramen on both sides opens anteriorly. On the left side, a small accessory foramen is positioned 7.4 mm superoposterior to the mental foramen, 21.8 mm above the base, 10.1 mm below the preserved alveolar margin, and it is open superiorly. Microcomputed tomography scans show that the canal of the small accessory foramen runs inferoposteriorly for ca. 8 mm before it merges with the mandibular canal. The oblique line extends anteriorly to the P_4 level and becomes more pronounced as it continues posteriorly and superoposteriorly to become continuous with the ramus root at the mid-M_2 level. The preserved anterior root of the ramus, set 8.8 mm lateral to the alveolar margin of the left M_2 at its distal end, makes a sharp superior bend at the mid-M_2 level and

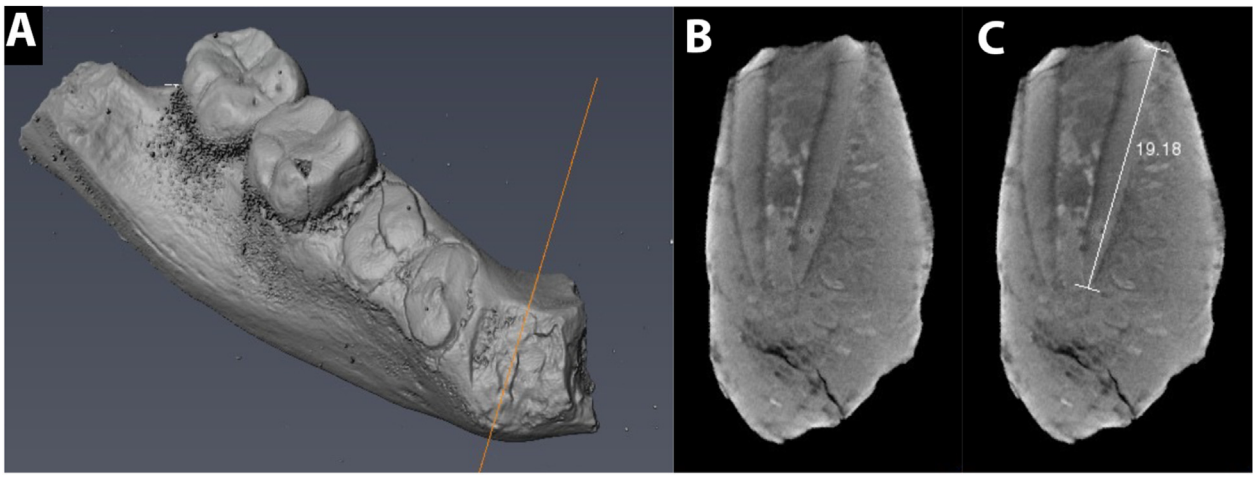

Figure 9. MSD-VP-5/16 canine root development. A) Surface model illustrating the plane of section through right mandibular canine alveolus for imaging canine development; B and C) ~19 mm of canine root development are present indicating the canine is likely between the developmental stage of root complete (R_c) and apex partially closed ($A_{½}$).

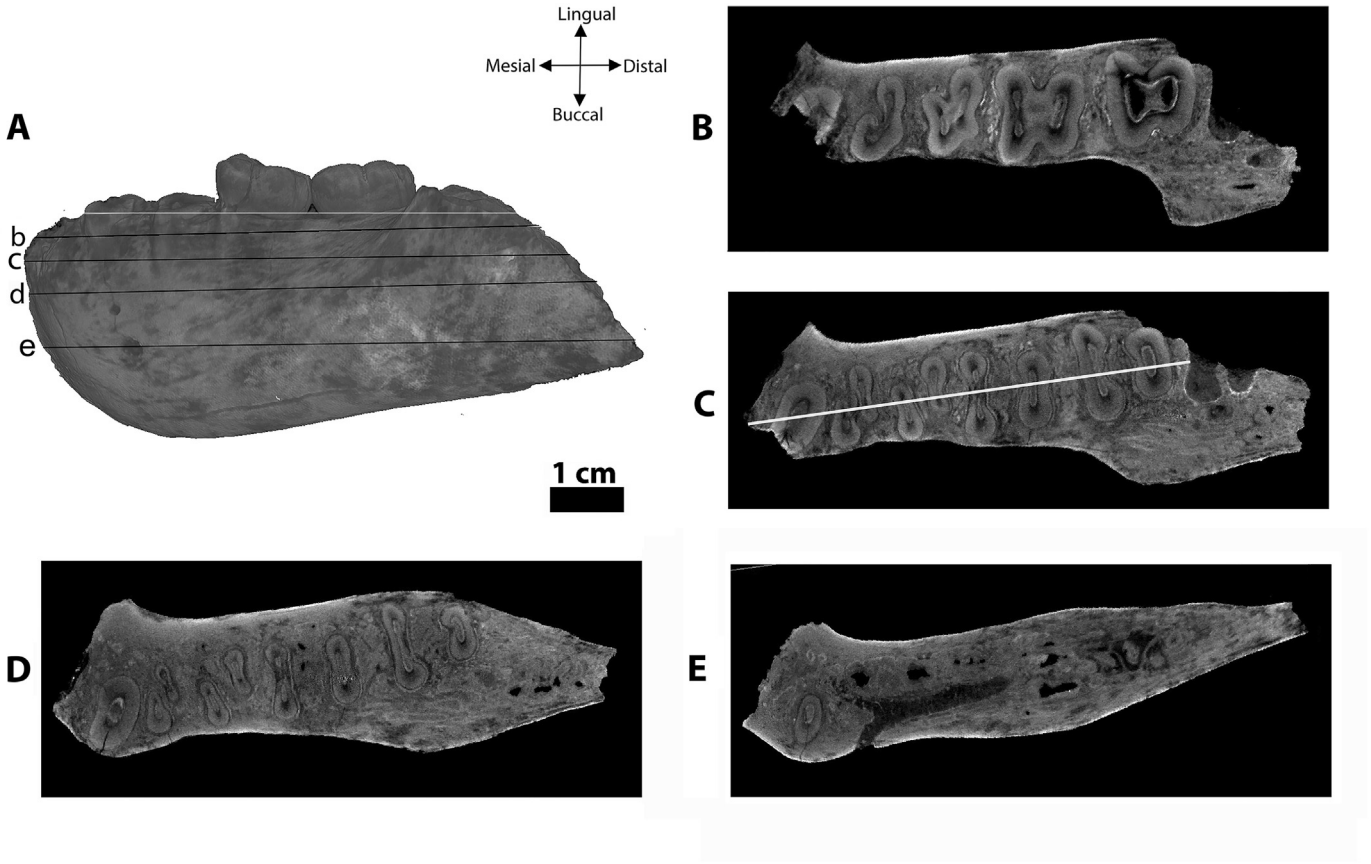

Figure 10. Premolar root cross-section of MSD-VP-5/16. A) surface model from μCT scan showing planes of sections used to generate B–E; B) ca. 2.9 mm; C) 5.9 mm (=mid-root level); D) 10 mm (=above the tip of the root); and E) at 17 mm below the approximated cervicoenamel junction (white line in A). Horizontal line in (C) shows the alignment of the C_1 with the postcanine teeth. The anatomical orientation legend applies to B–E.

obscures the distal M_2. The lateral prominence, positioned at the M_{1-2} level, is weakly expressed and its posterior margin gently blends with the shallow anterior inferior portion of the masseteric fossa. The corpus base is straight across its preserved length and its distal end shows no sign of ectoangular tuberosities.

Medial aspect The medial alveolar margin is preserved intact on the left side, from C_1 to mid-M_2, except for a small chip at the mesio-lingual corner of the M_1 root and minor indentations at the P_3 level (Fig. 3C). The left margin is undulating and not continuous at the C_1–P_4 level but becomes straighter, undisrupted, and rounder at

M_{1-2}. On the other hand, the margin is sharper on the right side, particularly at the M_{1-2}. Relatively weak juga can be palpated at the P_{3-4} medial alveolar margin on both sides. The alveolar prominence is rounded, especially at the M_{1-2} level. It is flatter but more expansive and diffuse at the level of the premolars. The mylohyoid line starts 7 mm from the alveolar margin at mid-M_2 to 15 mm inferior to the mid-M_1 alveolar margin. The subalveolar fossa is deep and extends from below the genioglossal fossa anteriorly, where it is the widest but shallower, to mid-corpus height extending to the level of distal M_2 (Fig. 3C). The inferior transverse torus, well developed all along its preserved length, bounds the subalveolar fossa inferiorly. This contributes substantially to the depth of the subalveolar fossa. This torus extends to the distal M_3 level where it is weaker but wider abruptly ending at the beginning of the depression for the attachment of the medial pterygoid muscle. A small groove runs out of the genioglossal fossa posteroinferiorly to the anterior portion of the subalveolar fossa. Numerous microforamina are present along the length of the inferior transverse torus with the largest located at the preserved distal end of the torus about 9 mm above the basal contour of the corpus. No endoangular tuberosities are present on the preserved distal end of the base.

Basal aspect The corpus base at the midline is slightly concave inferiorly. Lateral to the midline, the base becomes sharper and crest-like for 15 mm on the left and 9 mm on the right. The latter ends on a small tubercle that is absent on the left side. These sharp crests define the anterior edge of the digastric fossae, deeper and circular on the right side, and anteroposteriorly long on the left side. The corpus base contour posterior to the digastric fossae is rounded and evenly wide all the way to the M_2 where it begins to taper toward the base of the ascending ramus. Hairline cracks run across the corpus base on both sides although they do not affect any of the morphology.

3.3. Dental morphology of MSD-VP-5/16

Right fourth premolar The occlusal outline of this barely worn crown is a rounded square with a slight MD elongation. The tips of both protoconid and metaconid are polished and the mesial and distal marginal ridges are flattened by wear but no dentine is exposed. The presence or absence of a mesial interproximal facet cannot be verified with certainty due to enamel exfoliation and hairline cracks. The distal interproximal facet is convex and measures 3.2 mm BL. The protoconid is larger than the metaconid but they are of subequal height. The metaconid is set slightly mesial to the protoconid. The anterior fovea is an MD elongated slit-like shallow groove bounded mesially by the mesial marginal ridge and distally by the transverse crest connecting the protoconid and metaconid. Two vertical grooves descend to it from the mesial faces of the protoconid and metaconid. The transverse crest is truncated by the median longitudinal groove which runs from the anterior fovea to the slightly lingually positioned posterior fovea. The posterior fovea is positioned slightly more lingually and radial ridges lead to it from the distal face of the metaconid. A shallow groove on the occlusal surface separating the protoconid from a small distobuccal cuspule also runs to the posterior fovea. A thick distal marginal ridge bounds it distally. The buccal face of the tooth is convex transversely and vertically. It is narrow at its base but flares out toward the occlusal rim. The distal crest of the protoconid is much longer and more sloping than its mesial counterpart. The mesiobuccal groove is only a small pit positioned close to the occlusal rim. The distobuccal groove is obliterated by a small enamel chip but appears to have started at midcrown height and continues its course to the occlusal surface ending in the posterior fovea. The lingual face of the tooth is almost straight both vertically and transversely. Unlike the buccal side, the lingual crown face does not flare as much from the root to the occlusal rim. A central groove runs from mid-crown height to the occlusal rim. Another shallow groove 1.5 mm distal to it crosses the occlusal rim and ends in the posterior fovea. The root cross-section varies from two fused plate-like roots with four root canals a few mm below the cervicoenamel junction to two separate plate-like roots with four root canals at the midsection (Fig. 10A–E). In the P_3, the mesiobuccal and distal roots are separated at the midsection and the mesiobuccal root has a single rounded root canal while the distal root canal is plate-like. Cross-section at the level of the mental foramen (Fig. 10E) shows that the mandibular canal bifurcates anteriorly at the distal P_3 level to medial and lateral branches.

First molars Both sides are preserved but description is largely based on the more complete left side (missing only a small chip of enamel from the occlusal surface of the protoconid) supplemented with some observations on the right side (see Fig. 3G). The occlusal outline is a rounded rectangle with the distal half slightly narrower. The occlusal morphology is partly obliterated by moderate wear, but no dentine is exposed. A hairline crack passes along the MD length of the protoconid and hypoconid but does not affect observations of the occlusal morphology. The protoconid and metaconid are of equal size. The hypoconid is larger than the entoconid and the hypoconulid is the smallest cusp centrally positioned at the distal end of the crown. There are no accessory cuspules. The protoconid and hypoconid are polished flat and the entoconid is the least worn, still retaining its pointy tip, followed by the metaconid. The anterior and posterior foveae are obliterated by wear and only slit-like pits are remaining on both. Both foveae are set relatively lingually and the posterior fovea appears like a small groove on the distolingual corner of the crown. The central fovea is relatively shallow and positioned lingual to MD midline. The grooves separating the main cusps radiate to it. The median longitudinal groove zig-zags through the center of the crown, cutting through an entirely obliterated transverse crest connecting the protoconid and metaconid, traverses through the central fovea, and splits to form a Y-5 pattern with one branch separating the hypoconid from the hypoconulid and another branch ending in the posterior fovea. The lingual and buccal faces flare slightly occlusally. The lingual face is slightly bilobate as a result of centrally positioned mesial lingual groove that is shallow half way from the cervix and deeper closer to the occlusal rim. The buccal wall of the tooth is barely bilobate and when viewed mesially, the buccal contour of the tooth is relatively straight. A cingulum-like arc runs from the mesiobuccal corner close to the occlusal rim to the cusp divide at the center near the occlusal rim. The mesial interproximal facet is concave and wide, measuring 4 mm BL and 4 mm down from the occlusal rim. The distal interproximal facet measures at least 3.5 mm BL.

Left second molar The occlusal outline of the lightly worn crown is a mesiodistally elongate rectangle with rounded corners (Fig. 3F–G). It is morphologically similar to the M_1 but larger and relatively longer MD. The protoconid and metaconid are large and about the same size, followed by the sub-equal hypoconid, and entoconid. The hypoconulid is centrally positioned on the distal end of the crown clearly showing the arrangement of the major cusps in a Y-5 pattern. The tip of the protoconid and the mesial marginal ridge are polished flat with no dentine exposure. The tips of the other cusps are rounded. The lingual cusps are higher than their buccal counterparts. The groove that divides the buccal cusps on the occlusal surface is continuous in a straight line with the groove that divides the lingual cusps. This groove divides the crown into two subequal mesial and distal halves. The anterior fovea is divided into two portions due to wear on its central part. The buccal portion is a small pit on the mesiolingual corner of the protoconid and the slit-like lingual segment is positioned at the mesiobuccal

corner of the metaconid. The median longitudinal groove runs from the distal end of the anterior fovea posteriorly and bifurcates to a distobuccal and distolingual branches bounding the hypoconulid from the hypoconid and entoconid, respectively. Its distolingual branch ends in the posterior fovea which is a crescent-shaped fissure close to the distolingual corner of the crown. The lingual face is almost straight mesiodistally and superoinferiorly except for some MD convexity close to the mesiolingual and distolingual corners. The buccal face is bilobate and slopes occlusally more prominently above mid-crown height. Several shallow vertical grooves above mid-crown height create vertical ridges on the buccal face. The mesial buccal groove is the deepest and crosses the occlusal rim to continue to the center of the occlusal surface. What appears to be a remnant of a cingulum is present on the mesiobuccal corner. The mesial interproximal facet, 3.5 mm BL, is slightly concave and merges with the occlusal rim. There is no distal interproximal facet, suggesting that the M_3 was probably not in full occlusion.

3.4. Corpus morphology of MSD-VP-5/50

MSD-VP-5/50 is a left mandible with P_3–M_3. The anterior corpus is broken at the left I_2 level with the distal wall of the I_2 preserved. The canine root socket is present with some bone loss close to the alveolar margin. Based on the amount of wear on the molars, it is clear that it belonged to an adult individual (Fig. 5).

Occlusal aspect The mediolateral breadth of the corpus is almost uniform all along the postcanine tooth row, lacking substantial posterior thickening. The anterior to lateral corpus transition was more likely at C_1. Even though most of the lateral wall of the C_1 root socket is broken, what is preserved of the canine jugum at its base, combined with the lack of P_3 jugum, corroborates this inference. What can also be inferred from what is preserved around the symphyseal region is that the dental arcade was slightly divergent posteriorly. A small portion of the inferior transverse torus is preserved at the midline and extends posteriorly to the level of distal P_3.

Anterior aspect Some portion of the anterior corpus is preserved at the level of the I_2 and C_1. However, the midline point is difficult to determine despite some indications on the preserved superior and interiormost parts. The roughened surface below the I_2 and C_1 retreats posteroinferiorly toward the basal margin. What is preserved suggests that the symphyseal axis would have followed a similarly retreating path to the base. A slightly elevated area is palpable at the preserved bone at the level of the I_1.

Posterior aspect Only the edge of the inferior transverse torus at the transition to the lateral corpus is preserved and it is 17.1 mm superoinferiorly. The lateral edge of the genioglossal fossa is also preserved and clearly separates the superior transverse torus from the inferior transverse torus.

Lateral aspect The mesial half of the P_3 crown is slightly higher than the distal half, which is at the same level as the P_4. The P_4–M_3 row is straight and shows no sign of Curve of Spee or helicoidal tooth wear. The bone covering the lateral face of the C_1 root and the alveolar margin are entirely missing due to breakage and the nature of its jugum cannot be assessed. Based on the preserved root socket and the lingual face of the C_1 alveolus, the root was at least 24 mm long superoinferiorly. The C_1 to mesial M_2 alveolar margin is broken and corpus height at the level of these teeth cannot be measured accurately. However, it appears that corpus height was consistent across the postcanine tooth row even though the basal margin of the corpus is slightly convex. The height measured at P_3 from its cervicoenamel junction to the corpus base (45.6 mm) is almost identical to the height at M_1–M_2 (45.2 mm). It is slightly shorter at the M_3 level. The lateral face posterior to the P_3 does not show hollowing. It lacks a well-developed P_3 jugum. The mental foramen is positioned below mid-corpus height, 22.9 mm from the corpus base and 24.3 mm from the lowest point on the buccal cervicoenamel junction of the P_4, and opens anteriorly. It is anteroposteriorly elongated oval with sharp posterior edge and poorly defined anterior edge. Its superior and inferior edges are rounded. It is 2.6 mm superoinferiorly and 3.6 mm anteroposteriorly. There is a small shallow depression immediately behind it. An accessory foramen (1 mm superoinferiorly and 2 mm anteroposteriorly) is present at the level between P_3 and P_4, vertically 7.2 mm (actual diagonal distance is 9 mm) above the mental foramen, and opens superiorly. The lateral prominence is poorly developed and lies vertically at the level of the anteroinferior origin of the ascending ramus at mid-M_2. The extramolar sulcus is 12.1 mm, measured from the buccal face of the M_3 protoconid to the anterior edge of the ascending ramus, and runs anteroinferiorly.

The oblique line is not visible. The lower part of the corpus below the level of the mental foramen has three obliquely oriented platysmatic ridges anteriorly extending to below the C_1 root and ending in a well-defined, C-shaped groove. Posteriorly, these ridges end at the base of the corpus between P_3 and M_2. The area where the platysmatic ridges are present is the attachment area for the depressor anguli oris muscle. In lateral view, the corpus base is convex inferiorly with its most inferior point at M_1–M_2. It has a well-developed ectoangular tubercle close to the posterior end of the preserved base, which does not appear to be far from the missing gonial angle. The transition from the corpus base to the posterior edge of the ramus appears to have been arc-like even though some area above the gonial angle is broken.

The anterior origin of the ramus is set high, 11 mm below the M_2 alveolar margin and 34 mm from the base of the corpus, and its anterior edge runs obliquely in a superoposterior direction. The preserved anteroposterior width of the ramus at the occlusal plane is 58.6 mm. The mid-section of the masseteric fossa at this level is missing but enough of the fossa is preserved to indicate that the fossa was deep. The preserved height of the ascending ramus measured at its anterior edge perpendicular to the occlusal plane is 63.5 mm.

Medial aspect The alveolar margin is preserved intact only at the P_4–M_1 level and distal part of the M_3. It varies from sharp at P_4 and distal M_3 to rounded at M_1. There are multiple small foramina immediately below the alveolar margin of the P_4 and M_1 and posteriorly oriented grooves radiate out of them. The alveolar prominence is well developed, wide, and more pronounced anteriorly. It appears that it was continuous with the superior transverse torus anteriorly. Its posterior extent goes all the way to below the M_3 where it becomes a sharp ridge that curves posterolaterally to merge with the anterior medial edge of the ascending ramus. The mylohyoid groove runs obliquely immediately below the alveolar prominence and ends in the deep anterior portion of the subalveolar fossa. The posterior subalveolar fossa is shallow and it is posteriorly bounded by the anterior border of the medial pterygoid muscles. On the posteroinferior corner of the posterior subalveolar fossa, there is a prominent endoangular tubercle similar in size to the ectoangular tubercle on the buccal side. The inferior portion of the corpus below the subalveolar fossae is not bulging except for a slightly raised surface inferior to the deep anterior subalveolar fossa.

The bone surface of the triangular planum of the ascending ramus is largely missing but enough is preserved to show that it was deeply excavated. The preserved posterior and inferior portions of the ascending ramus show bony ridges and tuberosities for the medial pterygoid muscle. The retromolar fossa, medially bounded by a sharp ramus root, is 8.3 mm long anteroposteriorly.

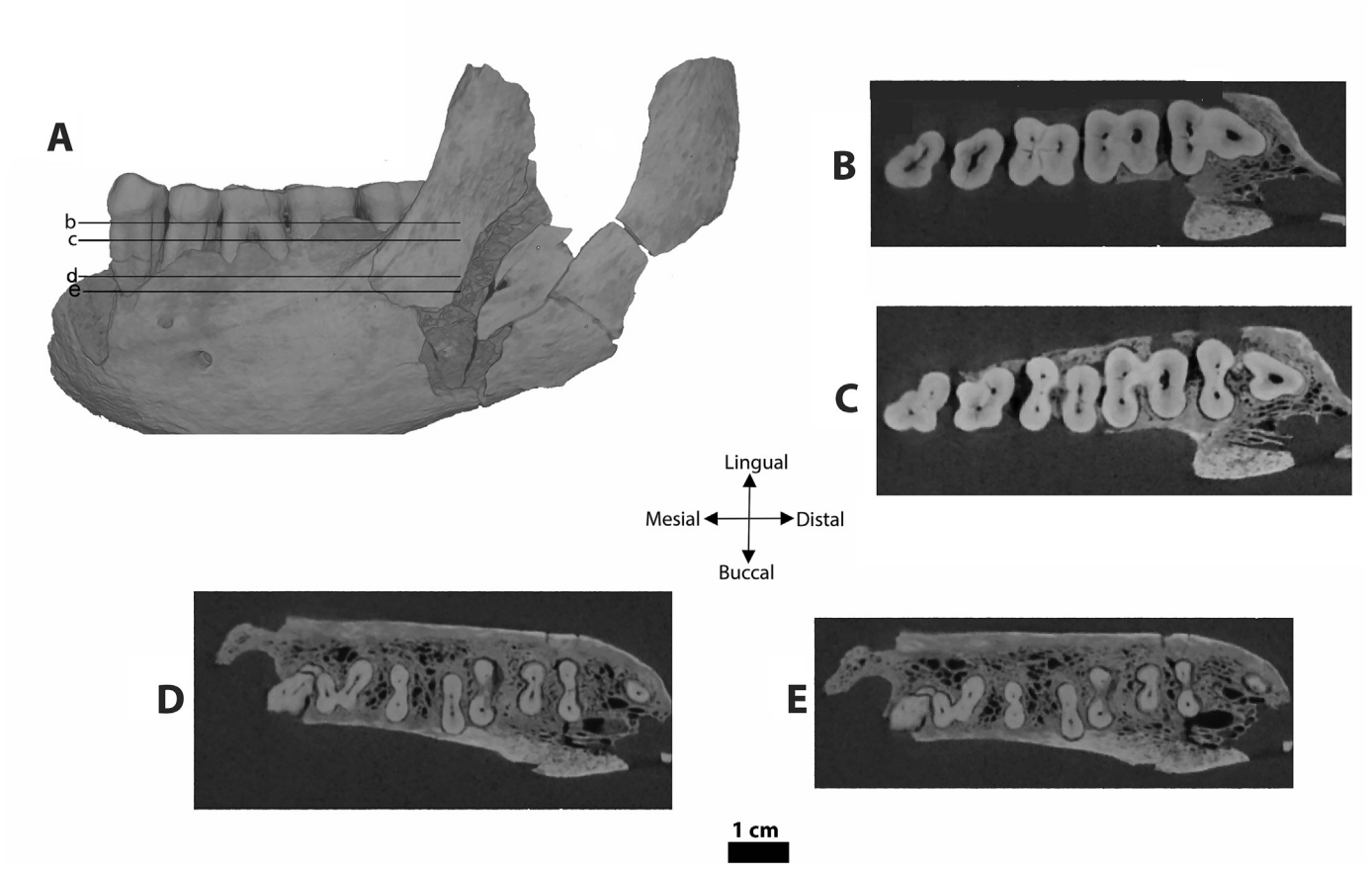

Figure 11. Premolar root cross-section of MSD-VP-5/50. A) Surface model from μCT scan showing planes of sections used to generate B–E; B) at approximated cervicoenamel junction; C) 2.8 mm below line b; D) 8.6 mm below line b; and E) 11 mm below line b. The anatomical orientation legend applies to B–E.

Basal aspect The corpus base is rounded for the most part and becomes thinner posteriorly until it becomes sharp posterior to the endo- and ectoangular tubercles. The digastric fossa is an anteroposteriorly elongated groove positioned lateral to the inferior transverse torus. Its lateral border is marked with prominent ridge that blends posteriorly to the corpus base. The medial edge of the corpus base below the posterior subalveolar fossa is sharp and merges with the endoangular tubercle.

3.5. Dental morphology of MSD-VP-5/50

Third premolar While some details of the occlusal morphology are slightly obliterated by wear, enough morphology is preserved to describe its overall shape and the size of its cusps. The occlusal outline of the crown is a mesiobuccal to distolingually elongated oval. The mesial half of the crown is higher than its distal half which is at the level of the P_4. The protoconid occupies most of the occlusal crown area and an incipient metaconid is present set low at a lingual terminus of the transverse crest. A narrow strip of dentine exposure runs from the protoconid tip distally along its distal crest for 4.5 mm. It is 0.9 mm wide at its widest on the protoconid tip. The buccal face slopes occlusally and it is mesiodistally convex with its mesial half facing more mesiobuccally. A shallow mesial buccal groove is present above mid-crown on the mesiobuccal corner and closer to the occlusal rim. The cervicoenamel junction is also set lower on the mesiobuccal corner. The slit-like anterior fovea is positioned on the mesiolingual corner of the crown. It is set high above the cervicoenamel junction, mesially bounded by a poorly defined but uninterrupted mesial marginal ridge formed by the mesial crests of the protoconid and incipient metaconid. The occlusal edge of the mesial marginal ridge is 4.2 mm above the cervicoenamel junction. The anterior fovea faces mesiolingually and slightly superiorly. The posterior fovea is also a short oblique hairline groove set at the bottom of a sloping surface descending from the distal protoconid crest. The distal marginal ridge is thick buccally and becomes thinner towards the distolingual corner of the crown where it merges with the distal metaconid crest. Most of the lingual face of the crown is vertical except for a small notch close to the occlusal rim separating the trigonid from the talonid. The mesial face of the crown does not show any sign of an interproximal facet, indicating a possible presence of a C_1/P_3 diastema. The distal interproximal facet is 4.2 mm BL (based on the dimension of the deeply concave interproximal facet of the P_4). The mesiobuccal and distal roots of the P_3, each with one root canal, remain connected across their entire length (Figs. 5C and 11).

Fourth premolar The occlusal crown outline is rhomboidal even though its basal crown outline is a mesiobuccal to distolingually elongated oval. Almost the entire occlusal surface is polished by wear. There is a small tear-drop-shaped dentine exposure close to the protoconid apex on the mesial side of the transverse crest. Two dot-like depressions—with no dentine exposure—are present behind the transverse crest lingual to the distal protoconid crest and on the lingual face of the metaconid apex. The transverse crest runs from the protoconid apex to the metaconid, distally bounding the entirely obliterated anterior fovea. The mesial interproximal

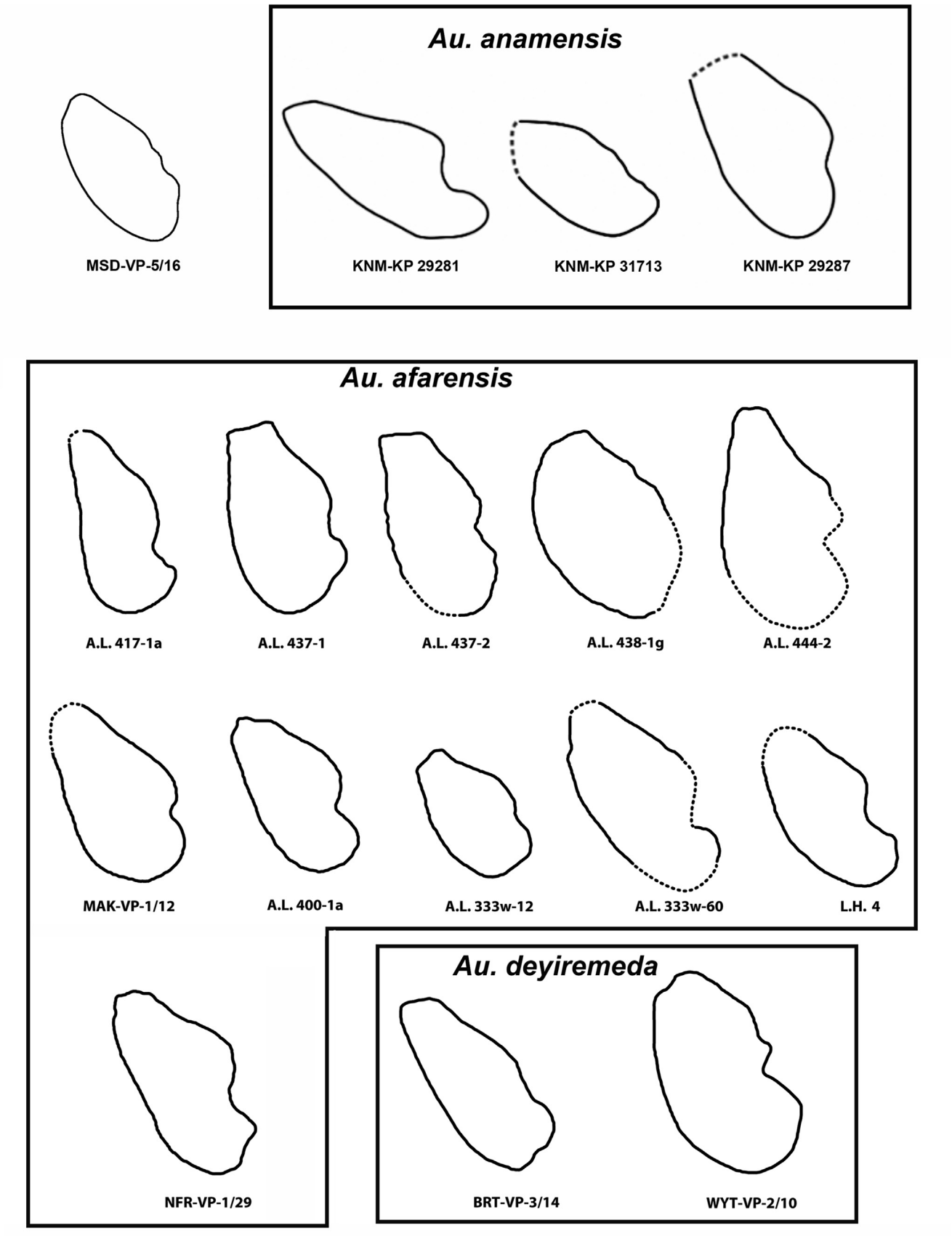

Figure 12. Symphyseal midsagittal contour of MSD-VP-5/16 taken perpendicular to the alveolar plane compared to contours of *Au. anamensis* ($n = 3$), *Au. afarensis* ($n = 11$), and *Au. deyiremeda* ($n = 2$) mandibles (not to scale). *Australopithecus anamensis* contours from Melillo et al. (2021); *Au. afarensis* contours (except NFR-VP-1/29) from Kimbel et al. (2004, Fig. 5.29), NFR-VP-1/29 from Haile-Selassie et al. (2015); *Au. deyiremeda* contours from Haile-Selassie et al. (2015). Dotted lines denote reconstructed contours.

facet is 4.2 mm BL. The posterior fovea is a slit-like groove centrally placed between the transverse crest and the distal edge of the crown. The distal interproximal facet is 3.9 mm BL. The lingual face is both MD and superoinferiorly straight except for the rounded mesial and distal corners. The buccal face is MD convex and slopes slightly occlusally with minimal flare in the same direction. The buccal crown bulge is positioned more mesially. The tooth has two fused roots, each with one root canal. The distal root is BL longer and offset lingually. These roots do not separate on the buccal side all the way to their tips (Fig. 11). The root morphology and number of root canals is similar to that of the P_3 although the mesial root of the P_4 is BL wider and the distal root more plate-like. The external root form remains the same for most of its entire length.

First molar This tooth is heavily worn. The buccal cusps show wide and deep dentine exposures stretching across the entire MD length of the crown. There is only an enamel rim left on its occlusal surface. The enamel on the mesiolingual face is missing. The crown outline is nearly square but slightly MD elongated. Its MD (corrected for interproximal wear) and BL dimensions are 12.2 mm and 11.9 mm, respectively. On the lingual side, the enamel is present on the occlusal surface only where the lingual groove cuts into the occlusal surface separating the metaconid and entoconid and on the distolingual corner of the distal marginal ridge. The enamel on the lingual wall of the metaconid is also spalled off. Almost the entire occlusal surface is heavily worn showing a deeply cupped dentine exposure running across its entire MD length. There is barely any enamel left on the mesial and distal marginal ridges. The occlusal area with exposed dentine is 10.7 mm MD with a minimum of 4.2 mm BL. As a result, the anterior, central, and posterior foveae are entirely obliterated. The mesial interproximal facet is mesially concave and 5.3 mm BL. The distal interproximal facet is slightly convex distally and 6.1 mm BL. The buccal face is bilobate and the buccal groove is set more mesially indicating that the protoconid was smaller than the hypoconid. The lingual groove, more prominent close to the occlusal rim, also indicates that the lingual face was also slightly bilobate and shows that the metaconid was much larger than the entoconid.

Second molar This tooth is also heavily worn but less so than the M_1. The enamel on the lingual face of the metaconid is spalled off. Like the M_1, the buccal cusps show wide and deep dentine exposures stretching across the entire MD length of the crown. However, there is still some enamel left on its lingual half. The metaconid occlusal surface has a circular dentine exposure that is larger (maximum diameter = 3.2 mm) than the one on the entoconid (maximum diameter = 2.1 mm). The occlusal outline of the crown is MD elongated rectangular with rounded corners. Its MD and BL dimensions (corrected for contact facets and loss of enamel surface) are 14.0 mm and 13.2 mm, respectively. The buccal half of the occlusal surface is heavily worn with deeply cupped dentine exposure along its entire MD length with only thin enamel rims remaining on the mesial and distal marginal ridges. As a result, the anterior, central, and posterior foveae are entirely obliterated. A large area of dentine is also exposed on the metaconid tip. The entoconid tip also has dentine exposure smaller than on the metaconid tip. The buccal face slopes slightly occlusally above mid-crown height and it is bilobate with a relatively deep buccal groove. The preserved lingual face distal to the lingual groove is convex, indicating that the face was bilobate. The mesial interproximal facet is concave mesially and 6.1 mm BL. The distal interproximal facet is almost straight and 6.3 mm BL.

Third molar This tooth is relatively less worn than the M_1 and M_2 even though it also has dentine exposures on the protoconid, hypoconid, and hypoconulid with the dentine cup on the latter cusp being the deepest and widest. The dentine exposure on the protoconid is still separate from those on the hypoconid and hypoconulid, which are connected. The occlusal outline is mostly MD elongated rectangle. However, its distal quarter is triangular with its distalmost end positioned at the distobuccal corner. Its MD and BL dimensions are 16.2 mm and 14.1 mm, respectively. The protoconid occlusal surface has a rectangular cupped dentine exposure measuring 4.2 mm MD and 2.7 mm BL. A diamond-shaped and cupped dentine exposure on the hypoconid merges distally with a deeply cupped dentine exposure on the buccal half of the hypoconulid cutting through the occlusal rim of the distal marginal ridge. The metaconid tip also has a small dentine exposure and the entoconid is worn flat with no dentine exposure. All of the occlusal foveae and contours are obliterated by wear except for remnants of the fissures separating the cusps. There might have been a small cuspule distal to the hypoconid. The lingual face is less bilobate and two shallow vertical grooves cross the occlusal rim separating the protoconid from the hypoconid and the latter from the hypoconulid. The buccal face slopes slightly occlusally and it is bilobate MD with the buccal groove positioned relatively mesially. The mesial interproximal facet is slightly concave mesially and 6.3 mm BL.

3.6. Comparative analysis

Our comparative sample for the analysis presented below includes the specimens listed in Table 1.

Corpus morphology Qualitatively, symphyseal inclination in MSD-VP-5/16 falls within the observed and highly variable range of *Au. afarensis* (Kimbel et al., 2004). In *Au. afarensis* mandibles, the anterior symphyseal contour and angulation is variable, ranging from fairly vertical (e.g., A.L. 288-1, A.L. 417-1) to relatively inclined (e.g., A.L. 400-1, A.L. 277-1, MAK-VP-1/12), but frequently associated with a rounded and bulbous inferior portion (Kimbel et al., 2004; Fig. 12). However, the holotype mandible of the species (L.H. 4) has been described as different from other mandibles of the species in terms of the morphology of its external symphyseal contour. In L.H. 4, while its overall inclination is within the range of the Hadar mandibles, the inferior half of its contour in not bulbous but rather continuously retreating posteriorly (White, 1977; Kimbel et al., 2004). The overall external contour of MSD-VP-5/16 is more like L.H. 4 (Fig. 12), where the basal portion of its symphysis recedes more extensively than its superior half (Kimbel et al., 2004). Although the symphysis of MSD-VP-5/50 at the midline is broken, the preserved portions of the anterior corpus and cross-section at P_3 (Fig. 13) indicate that the external contour of its symphysis was more strongly inclined than in MSD-VP-5/16. The degree of posteroinferior and inferomedial retreat in the preserved anterior corpus of MSD-VP-5/50, particularly in the P_3 area, indicates that it had an extremely receding symphyseal axis (see Figs. 5E and 13). The external contour of the symphysis in known *Ar. ramidus* and *Ar. anamensis* mandibles is also extremely receding (White et al., 1994, 2009; Leakey et al., 1995; Ward et al., 2001). The cross-sections of some *Au. anamensis* mandibles at the distal P_3 level show that the inferior one-third of the lateral profile sharply sweeps inferomedially. This lends support to the inference made on the degree of symphyseal inclination in MSD-VP-5/50. The symphyseal external contour in *Au. deyiremeda* mandibles falls within the range of *Au. afarensis* variation. The degree of inclination in MSD-VP-5/16 is similar to the *Au. deyiremeda* mandible (WYT-VP-2/10), which

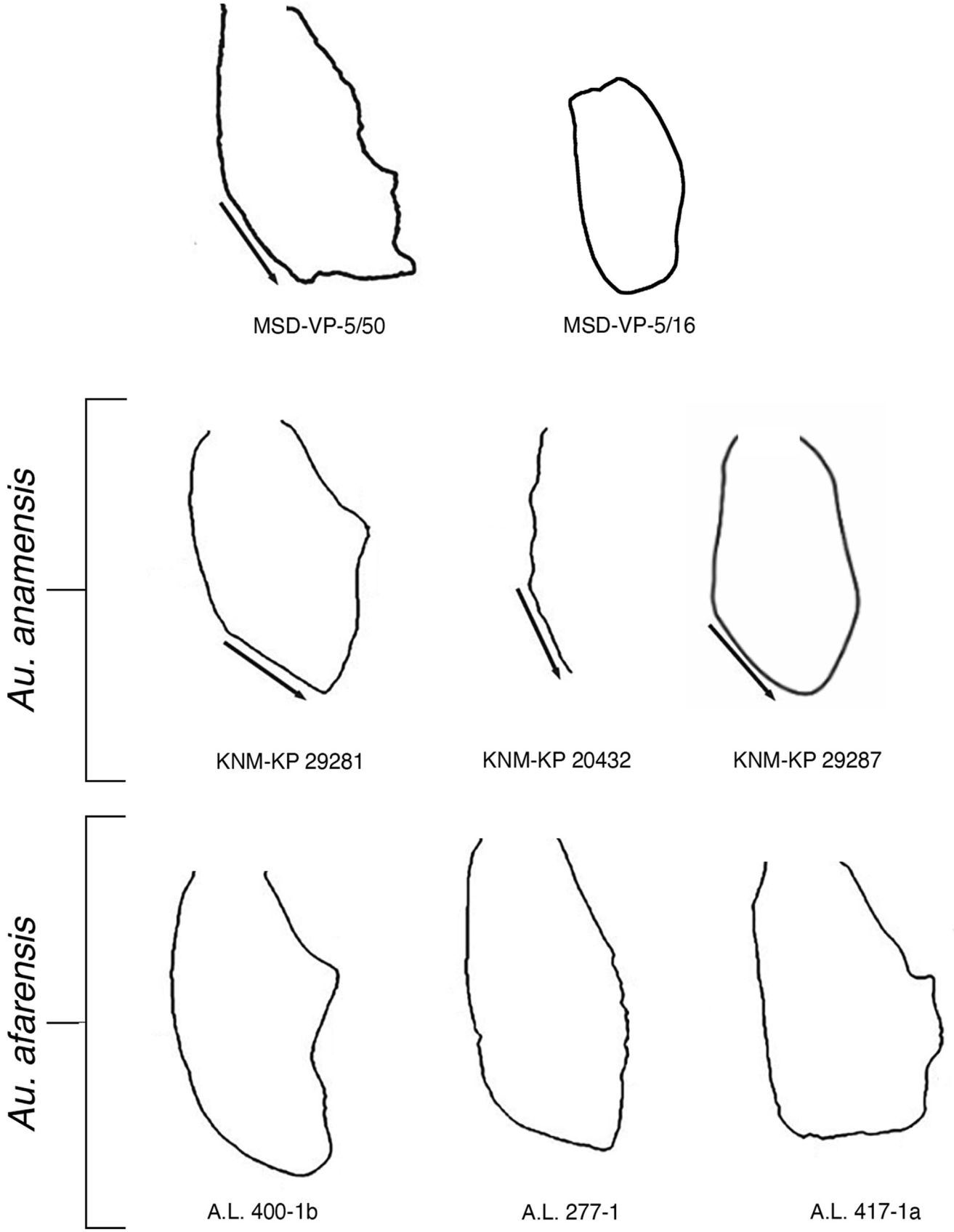

Figure 13. Mandibular corpus cross-sections at distal P_3 (MSD mandibles, *Au. anamensis*, and *Au. afarensis*). Note that MSD-VP-5/50 has a cross-section similar to *Au. anamensis*, while MSD-VP-5/16 resembles those of *Au. afarensis* in having a vertical lateral wall all the way to its base. Modified from Kimbel et al. (2006) and Haile-Selassie (2010).

also resembles the holotype of *Au. afarensis* (L.H. 4; Haile-Selassie et al., 2015).

The anterior-to-lateral corpus transition in MSD-VP-5/16 is clearly at the C_1s while the transition in MSD-VP-5/50 can only be inferred as at C_1, based on the estimated lateral extent of the broken C_1 jugum and corpus morphology at the P_3 level (Fig. 5). The dental arcade of MSD-VP-5/16 and MSD-VP-5/50 appears to have been slightly divergent posteriorly (comparable to A.L. 400-1), even though the anterior to posterior corpus transition in both specimens is at the C_1s. Based on published images, the transition in *Ar. ramidus* appears to be at the C_1s and also had parallel tooth rows (Figure 4 in White et al., 2009). The transition in *Au. anamensis* mandibles is at the C_1s, and the alveolar arch is U-shaped with relatively parallel tooth rows (Fig. 14). This is one of the few characters that distinguishes *Au. afarensis* from *Au. anamensis* (Leakey et al., 1995; Ward et al., 2001). In *Au. afarensis*, the anterior-to-lateral corpus transition is usually at P_3 or combined C/P_3 jugum and the postcanine tooth rows are divergent posteriorly (Kimbel et al., 2004). In the two known mandibles of *Au. deyiremeda*, the transition is either at C_1 (WYT-VP-2/10) or mesial P_3 (BRT-VP-3/14) and the tooth rows are slightly divergent posteriorly as seen in the latter specimen (Fig. 14).

The presence of a distinct lateral corpus contour hollow, posterior to the C_1/P_3 jugae, has been described as typical and characteristic of both *Au. anamensis* and *Au. afarensis* mandibles (White et al., 2000; Kimbel et al., 2004). A shallow lateral depression is also present in MSD-VP-5/16 posterior to the C_1 jugum while it is almost nonexistent, or poorly defined and barely palpable in MSD-VP-5/50. The anteroposterior extent and depth of the hollow in MSD-VP-5/16 is comparable to *Au. afarensis* specimens such as A.L. 288-1. In *Au. afarensis*, the hollow is anteriorly bound by a P_3 or combined C_1–P_3 jugum—which also defines the anterior to lateral corpus transition—positioned below the premolars superior or superoposterior to the mental foramen (Kimbel et al., 2004). In MSD-VP-5/16, it is bounded anteriorly by a laterally bulging C_1 jugum while its posterior boundary is poorly defined. In the two known *Au. deyiremeda* mandibles, the lateral corpus is extremely inflated and is lacking a lateral corpus hollow (Haile-Selassie et al., 2015).

In terms of corpus shape (robusticity), *Au. anamensis* mandibles have been characterized as less robust than in *Au. afarensis* (Ward et al., 2001), even though more recent discoveries indicate that there is considerable variation in mandibular size and shape in both species (Ward et al., 2020). Mandibular corpus cross-section of both *Au. anamensis* and *Au. afarensis* at the M_1 level clearly shows this variability (Fig. 15). Even in earlier species such as *Ar. ramidus*, corpus shape is variable from deep and narrow in ARA-VP-6/500 from Aramis (White et al., 2009) to shallow and broad in GWM3/P1 from Gona (Semaw et al., 2005). In *Au. afarensis*, although there is clear evidence from Hadar that mandibles of the species become larger through time—particularly in terms of corpus height—the change in overall shape is not statistically significant (Lockwood et al., 2000). The corpus height of MSD-VP-5/50 (measured at the level of M_1) exceeds the maximum documented for both *Au. anamensis* and *Au. afarensis*, whereas its breadth is within the range of *Au. afarensis* (Table 3). However, in terms of its corpus shape, it falls outside the documented lower value in both *Au. anamensis* and *Au. afarensis*, indicating that its corpus is relatively compressed bilaterally and long in the superoinferior dimension. On the other hand, although the corpus height and breadth in MSD-VP-5/16 fall within the range of both *Au. anamensis* and *Au. afarensis*, its shape falls outside the range of *Au. anamensis* and on the higher end of *Au. afarensis*, indicating that its corpus is robust despite its overall small size (Table 3).

Compared to known mandibles of *Au. deyiremeda* ($n = 2$), the corpus height in MSD-VP-5/16 is slightly lower while that of MSD-VP-5/50 is markedly higher. However, the corpus breadth and shape in the Woranso-Mille mandibles are lower than both *Au. deyiremeda* mandibles (Table 3). Overall mandibular corpus morphology in *Au. deyiremeda* appears to noticeably depart from that of *Ar. ramidus*, *Au. anamensis*, and in some ways from that of *Au. afarensis* (Haile-Selassie et al., 2015). Its corpus is more robust, like species of the genus *Paranthropus*, and lacks some of the features that have been identified as typical of *Au. afarensis*. Although a scatterplot of corpus height vs. breadth in *Au. afarensis* mandibles ($n = 24$) shows a slightly scattered distribution, the correlation between the two variables is significant ($r = 0.60$, $p < 0.01$; Fig. 16A). Furthermore, all of the *Au. afarensis* specimens fall within the 95% CI. When the *Au. anamensis* ($n = 3$) specimens are added to the *Au. afarensis* data set, the correlation and *p*-value are almost the same (Fig. 16B), and the *Au. anamensis* specimens fall within the 95% CI of *Au. afarensis*. Inclusion of the two Woranso-Mille mandibles into the combined *Au. anamensis* and *Au afarensis* data set slightly reduces the correlation coefficient ($r = 0.57$) but the *p*-value remains the same (Fig. 16C). However, MSD-VP-5/50 falls outside the 95% CI of *Au. afarensis*. On the other hand, when the two *Au. deyiremeda* mandibles are included in the combined data set, the correlation, though still significant ($p < 0.01$), reduces to 0.47 and they fall outside the 95% CI of *Au. afarensis* (Fig. 16D). While there is clearly a significant correlation between the height and breadth of mandibular corpus at M_1, it appears that the correlation coefficient and *p*-value are influenced by the specimens included in the analysis. However, we find it interesting to see that while the *Au. anamensis* specimens fall within the *Au. afarensis* 95% CI, MSD-VP-5/50 and the two *Au. deyiremeda* mandibles fall outside that interval. This could be due to the markedly high corpus height of MSD-VP-5/50 and more robust nature of the *Au. deyiremeda* mandibles.

Morphology of the ramus MSD-VP-5/50 preserves most of the anterior and some part of the posterior margin of the ramus that can be qualitatively assessed and compared to *Ar. ramidus*, *Au. anamensis*, *Au. afarensis*, and *Au. deyiremeda*, particularly in terms of the orientation of these margins and the size of the extramolar sulcus. What is preserved of the corpus base and the posterior margin of the ramus in MSD-VP-5/50 is also adequate to reconstruct the curvature along its gonial angle. As mentioned in the description, MSD-VP-5/50 has an anterior ramus margin that is oriented obliquely superoposteriorly. The preserved superior half of the posterior margin also shows similar orientation (Fig. 17). The anterior origin of the ramus is set high at the mid-M_2 level and when viewed laterally it does not obscure the M_2. In contrast, the anterior ramus margin of MSD-VP-5/16 obscures the distal portion of the M_2 (Fig. 3B). In MSD-VP-5/50, the transition from the corpus base to the posterior edge of the ramus also appears to have been arc-like even though the gonial angle is broken (see Fig. 17).

Ramus morphology in *Ar. ramidus* is unknown from the type locality Aramis (White et al., 2009). However, based on published figures (Fig. 2 in Suwa et al., 2009b), the ramus root in *Ar. ramidus* mandibles such as ARA-VP-1/401 and ARA-VP-6/500 appears to have been set high and placed posteriorly. Furthermore, also based on published images (Semaw et al., 2005; White et al., 2009; Suwa et al., 2009b) and observations on original specimens (Aramis material only), the anterior edge of the ascending ramus in ARA-VP-6/500 and ARA-VP-1/401 does not seem to obscure the M_2, and both mandibles have relatively small extramolar sulci. Morphology of the ramus in *Au. anamensis* mandibles is poorly known to fully assess the orientation of the anterior and posterior margins of the ramus. However, in the holotype mandible of *Au. anamensis* (KNM-

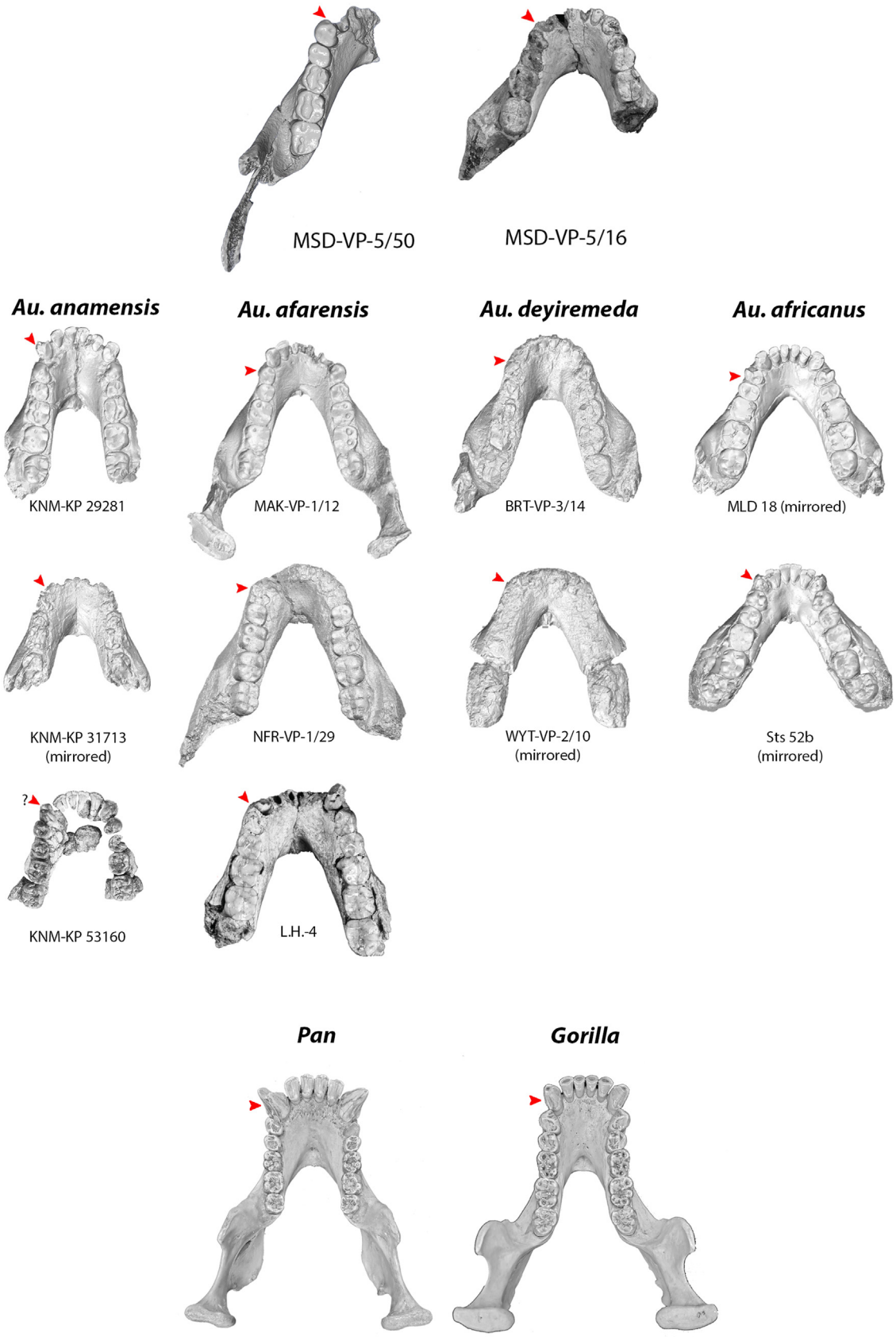

Figure 14. Comparison of the location of the anterior to lateral corpus transition (indicated by red arrows) in the MSD mandibles, *Au. anamensis*, *Au. afarensis*, *Au. deyiremeda*, *Au. africanus*, and the African apes. Note that the point of transition in the two MSD mandibles is at the canine, as in *Au. anamensis* and the African apes, while the transition in the other species is at, or posterior to the P_3. (For interpretation of the references to color in this figure legend, the reader is referred to the Web version of this article).

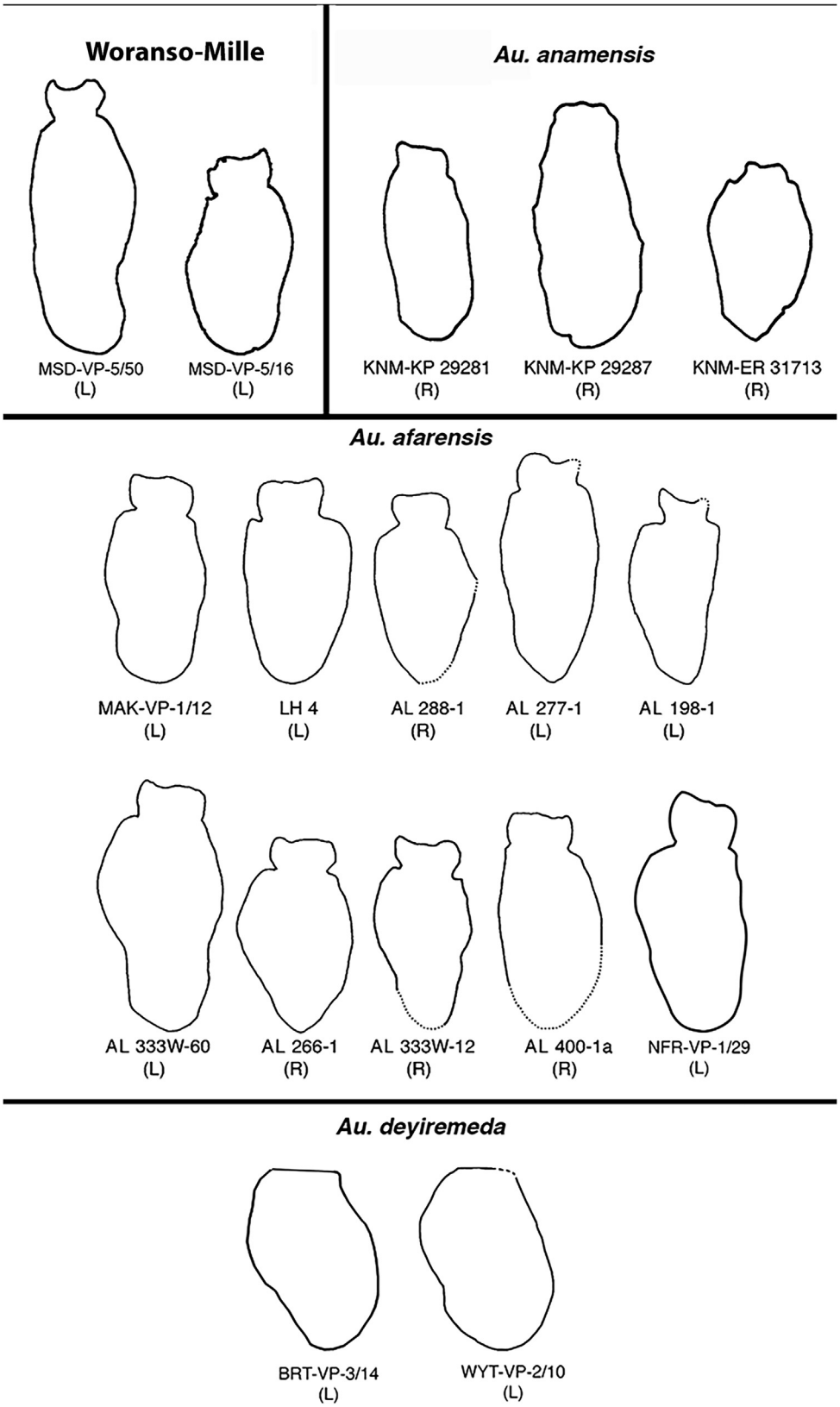

Figure 15. Mandibular corpus cross-sections of the Woranso-Mille specimens, *Au. anamensis* and *Au. afarensis* at mid-M_1 level, perpendicular to the alveolar plane. Dotted lines indicate reconstructed areas. Cross-sections of the *Au. afarensis* and *Au. anamensis* mandibles are from White et al. (2000, their Fig. 10) and Ward et al. (2001, their Fig. 27), respectively.

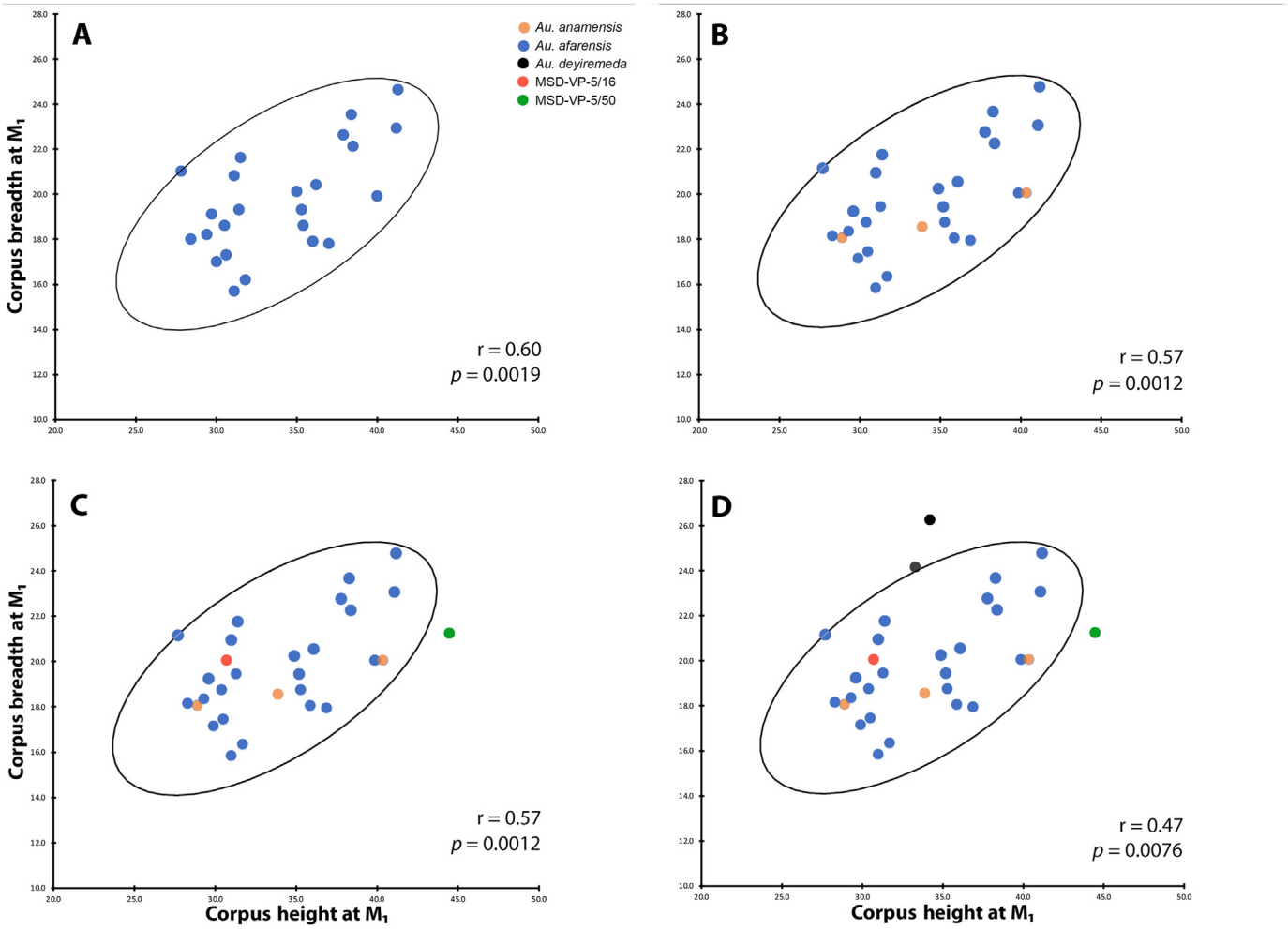

Figure 16. Bivariate scatterplot of mandibular corpus height and mandibular corpus breadth at mid-M_1 level. The ellipse in each panel indicates 95% CI for *Au. afarensis* only. The Pearson's correlation coefficient (r) and *p*-values are calculated for: A) *Au. afarensis* only; B) *Au. afarensis* and Woranso-Mille mandibles; C) *Au. anamensis*, *Au. afarensis*, and Woranso-Mille mandibles, and D) *Au. anamensis*, *Au. afarensis*, *Au. deyiremeda*, and Woranso-Mille mandibles combined (see text for details). Metric data for the comparative species was compiled from White (1977), White et al. (2000), Ward et al. (2001, 2013, 2020), Kimbel et al. (2004), Haile-Selassie et al. (2016b), and Melillo et al. (2021).

KP 29281) and in KNM-KP 31713, the ramus root is set high and takes its origin at the mid-M_2 level (Figs. 17 and 18). In *Au. afarensis* mandibles, there is enough evidence to indicate that the anterior and posterior margins of the ramus are vertically oriented and the anterior origin of the margin is mostly at mid-corpus height (White et al., 2000; Rak et al., 2007). The A.L. 822-1 mandible from Hadar has the most complete ramus (Rak et al., 2007), and clearly shows this condition. In contrast, MSD-VP-5/50 shows posteriorly inclined anterior and posterior margins (Fig. 17). This configuration is prevalent among chimpanzees but not in gorillas (White et al., 2000; Rak et al., 2007). Furthermore, in *Au. afarensis* mandibles where the anterior ramus margin is preserved, the ramus, in lateral view, obscures the entire (MAK-VP-1/2 and -1/12, A.L. 822-1), or one-half to two-thirds (A.L. 444-2) of the M_2 (White et al., 2000; Kimbel et al., 2004; Rak et al., 2007). The only exception is A.L. 198-1, where the ramus obscures only the distal half of the M_3, a condition similar to MSD-VP-5/50. MSD-VP-5/16, on the other hand, is like most *Au. afarensis* mandibles. The ramus obscures the distal half of the M_2 and the anterior origin of the margin is at mid-corpus height. The paratype mandibles of *Au. deyiremeda* do not preserve enough of the ascending ramus to confidently characterize the orientation of the anterior edge. However, based on what is preserved on the left side of BRT-VP-3/14, it appears to have been more vertical than in MSD-VP-5/50. The origin of the anterior margin of the ramus in this mandible is also set at mid-corpus at P_4 level and obscures the distal half of the M_2 (Haile-Selassie et al., 2015). In MSD-VP-5/50, the anterior margin of the ramus obscures only the distal one-third of the M_3. While considerable interspecific variation in the anterior origin of the ramus is apparent, chimpanzees have posteriorly inclined anterior and posterior ramus margins, have a high and posteriorly placed ramus root, and the ramus does not obscure the M_2, indicating that these features could be plesiomorphic to hominins (see Figs. 17 and 18).

Dentition Qualitative assessment shows that the occlusal outline of the premolar crowns and the number of their roots in the MSD mandibles differ from what has been described as characteristic of *Ar. ramidus* (e.g., single-rooted P_4). The P_3 of MSD-VP-5/50 is similar to some *Ar. ramidus* P_3s in being obliquely elongate but it is not unicuspid in the same way and lacks a mesially open anterior fovea. *Au. anamensis* has unicuspid P_3 associated with mesially open anterior fovea even though one *Au. anamensis* P_3 from Allia Bay (KNM-ER 20432) has an incipient metaconid and a crown shape and morphology more similar to *Au. afarensis* than to *Au. anamensis* (Kimbel et al., 2006; Delezene and Kimbel, 2011). A considerable amount of variation is also present in *Au. afarensis* P_3s (Delezene and Kimbel, 2011; Delezene et al., 2013). Despite such variation,

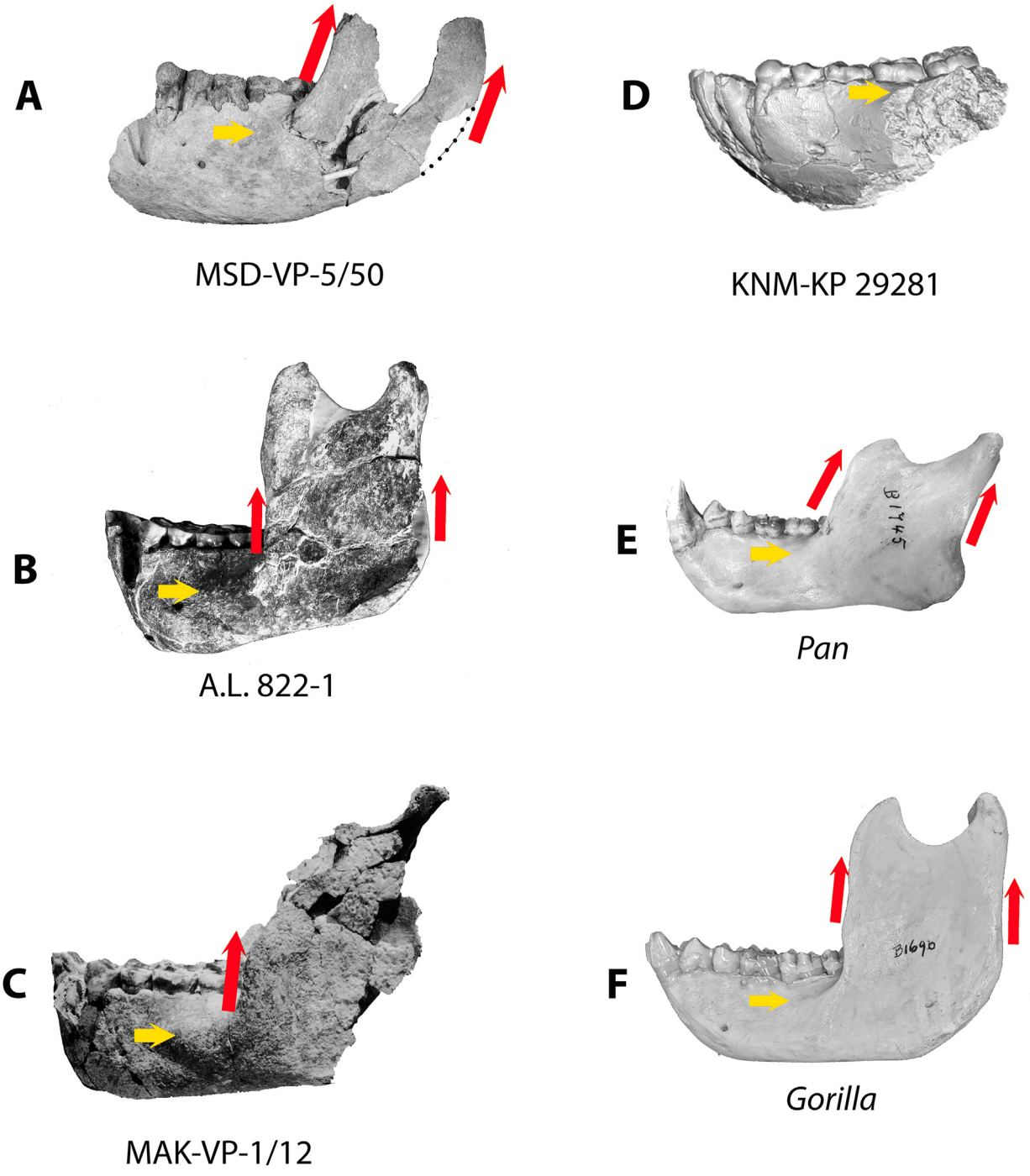

Figure 17. Lateral views of MSD-VP-5/50 (A); *Au. afarensis* mandibles A.L. 822-1 (B) and MAK-VP-1/12 (C); *Au. anamensis* mandible KNM-KP 29281 (D); *Pan troglodytes* (E) and *Gorilla gorilla* (F) mandibles, showing the anterior and posterior margins of the ramus (red arrows) and location of the anterior origin of the ramus relative to the height of the corpus (yellow arrows). Images B and C were modified from Rak et al. (2007) and White et al. (2000), respectively. Specimens are not to scale. See text for discussions.

however, the mesial border of the anterior fovea in most *Au. afarensis* P_3s is demarcated by a well-developed and undivided mesial marginal ridge, with the exception of probably a few P_3s that have mesially open anterior fovea (e.g., A.L. 128-23). While the occlusal outline and absolute sizes of the anterior and posterior foveae of MSD-VP-5/50 P_3 tend to be similar to some *Au. anamensis* P_3s, its anterior fovea/posterior fovea ratio is much lower than in known *Au. anamensis* P_3s (Delezene and Kimbel, 2011), mainly due to its more mesiolingually oriented mesial protoconid crest. The one known P_3 of *Au. deyiremeda* (BRT-VP-3/14) also has a mesially open anterior fovea with a truncated mesial marginal ridge. However, it also has a well-developed metaconid unlike MSD-VP-5/50 and it is also higher crowned.

The occlusal outline of the P_4 crowns of MSD-VP-5/50 and MSD-VP-5/16 are rhomboidal with an extremely bulging distolingual corner or a rounded square, respectively, and have two fused roots varying in cross-section from the cervical to the apical end (Figs. 10 and 11). In *Ar. ramidus*, the P_4s have ovoid occlusal crown outlines

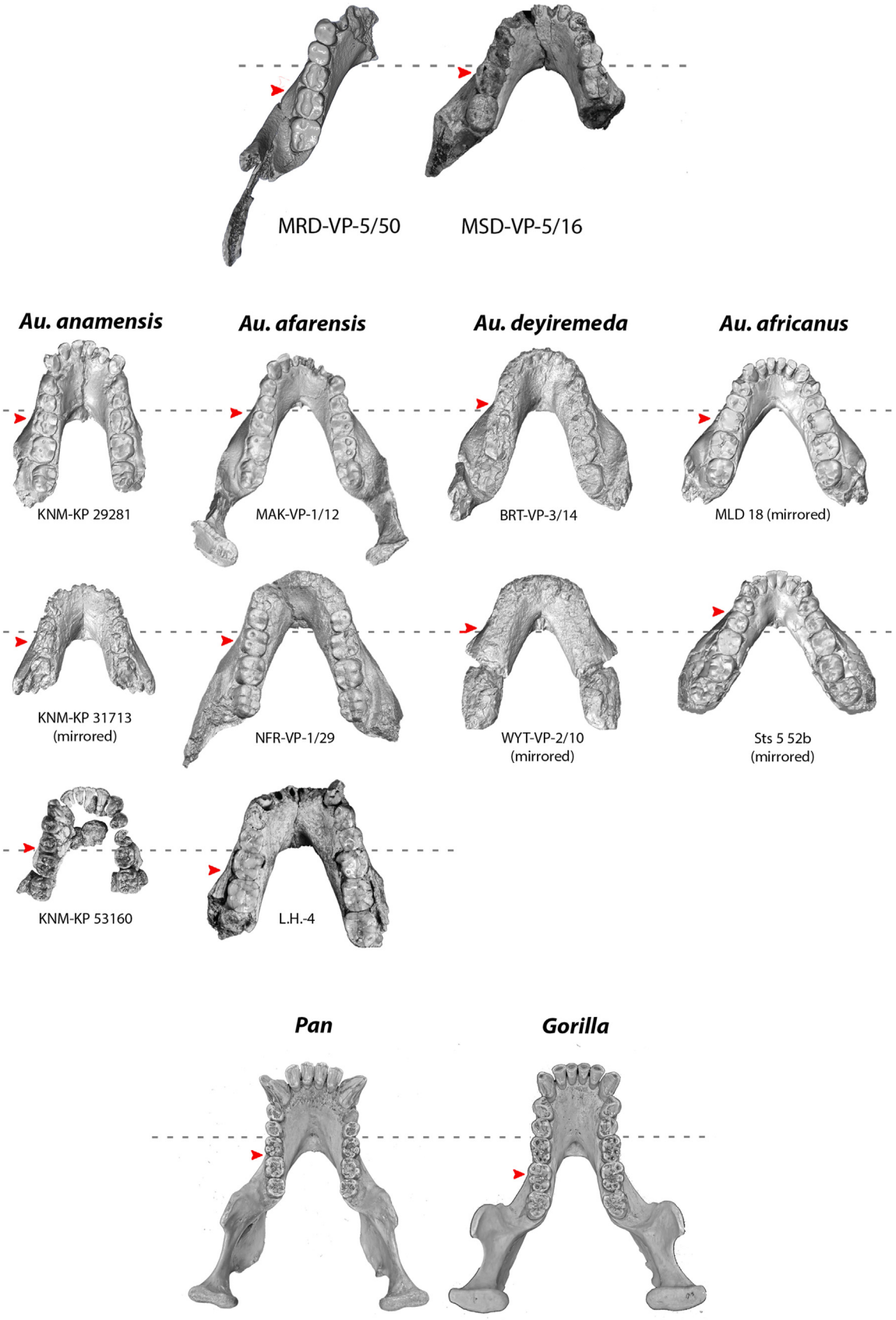

Figure 18. Occlusal views of MSD-VP-5/16, MSD-VP-5/50, *Au. anamensis*, *Au. afarensis*, *Au. deyiremeda*, and *Au. africanus*, *Pan troglodytes*, and *Gorilla gorilla* mandibles showing the anterior origin of the ramus (red arrow). Dashed line runs across the distal P_4. Specimens are not to scale. (For interpretation of the references to color in this figure legend, the reader is referred to the Web version of this article).

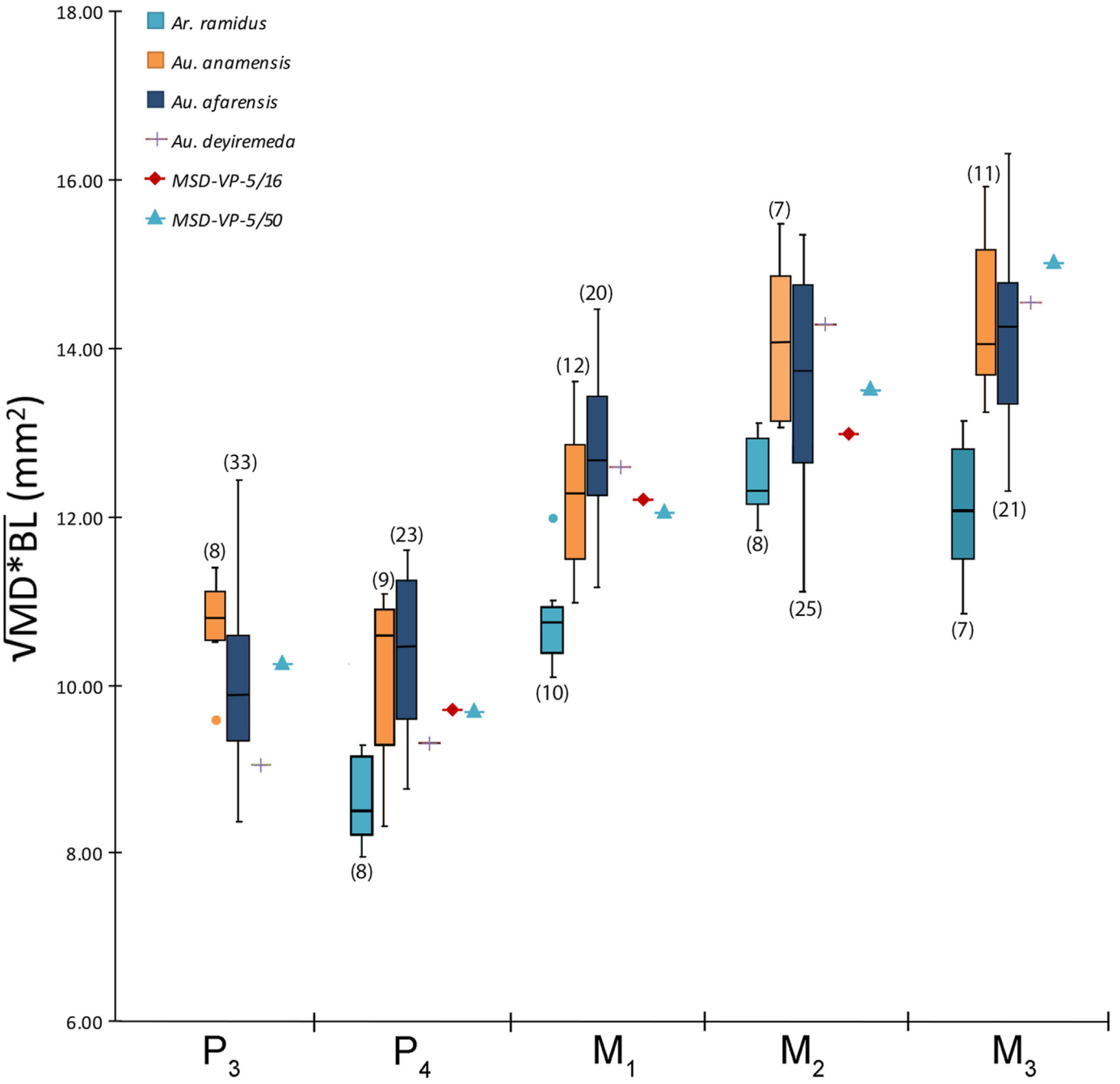

Figure 19. Box-and-whisker plot of P_3–M_3 crown area ($\sqrt{}$MDxBL) comparing MSD-VP-5/16 and MSD-VP-5/50 with *Ar. ramidus* (P_3 not included), *Au. anamensis*, *Au. afarensis*, and *Australopithecus* specimens from Woranso-Mille. Horizontal line within each box is the median, lower and upper ends of each box represent the first and third quartiles, respectively, and the ends of the whiskers represent ±1.5 × interquartile range. Points above or below the ends of the whiskers of each taxon represent outliers. Measurements of the comparative species were compiled from White (1977), Ward et al. (2001, 2013, 2020), Kimbel et al. (2004), Semaw et al. (2005), Haile-Selassie et al. (2015), White et al. (2015), Haile-Selassie and Ryan (2019), and Melillo et al. (2021).

associated with a single root (White et al., 1994; Semaw et al., 2005; Suwa et al., 2009a). Most *Au. anamensis* P_4s have predominantly trapezoidal or rhomboidal occlusal crown outlines (Ward et al., 2001) even though there are some P_4s with an oval outline (Ward et al., 2013). In *Au. afarensis*, although there is considerable variation, most P_4s in this species have rounded square occlusal outlines (White, 1977; Johanson et al., 1982), even though an oval outline is apparent in some specimens (e.g., EP 2400/00, L.H. 3; Leakey, 1987; Harrison, 2011). The number of roots on the P_4s of these two australopiths is also variable but they all have multiple roots, unlike *Ar. ramidus*. The P_4 anterior fovea in both MSD mandibles is smaller than the posterior fovea, similar to *Au. afarensis* P_4s. However, *Ar. ramidus* and *Au. anamensis* P_4s have relatively large anterior fovea compared to the posterior fovea.

The MSD mandibles and teeth overlap in several metric variables with almost all of the comparative taxa. However, there are also some differences, particularly in individual tooth size and shape and corpus depth. The occlusal crown area of the preserved teeth in MSD-VP-5/50 and MSD-VP-5/16 are larger for most postcanine positions than those of *Ar. ramidus* (Fig. 19) and the

Table 4
Premolar dimensions of *Au. anamensis* and *Au. afarensis*. The list includes specimens that have both premolars preserved. Mesiodistal (MD) and Buccolingual (BL) measurements (mm) were compiled from White (1977), Leakey et al. (1995), Ward et al. (2001, 2013, 2020), Kimbel et al. (2004), White et al. (2000), Harrison (2011), Haile-Selassie and Ryan (2019), and Melillo et al. (2021).

Specimen	P_3			P_4			Ratio[a]
	MD	BL	Area $\sqrt{MD*BL}$	MD	BL	Area $\sqrt{MD*BL}$	
MSD-VP-5/50	10.4	10.1	10.25	9.1	10.3	9.68	**105.89**
Au. anamensis							
KNM-ER 20432	9.7	11.4	10.52	10	11.7	10.82	97.23
KNM-KP 29281	9.3	9.9	9.60	8.2	9.8	8.96	**107.14**
KNM-KP 29286	10.3	11	10.64	9.6	11.7	10.60	**100.38**
KNM-KP 47953	9.4	13.4	11.22	9.4	12.8	10.97	**102.28**
KNM-KP 53160	10.3	11.3	10.79	9.9	9.5	9.70	**111.24**
Au. afarensis							
A.L. 128-23	8.2	9.6	8.87	7.7	10.0	8.77	**101.11**
A.L. 198-1	9.4	9.5	9.45	8.9	9.8	9.34	**101.19**
A.L. 207-13	8.8	9.5	9.14	9.2	10.0	9.59	95.33
A.L. 266-1	9.4	10.7	10.03	9.7	10.7	10.19	98.44
A.L. 277-1	9.6	12.3	10.87	10.4	11.8	11.08	98.09
A.L. 288-1i	8.4	10.0	9.17	8.2	10.5	9.28	98.77
A.L. 333w-.1	9.7	10.3	10.0	9.5	10.5	9.99	**100.08**
A.L. 333w-32	9.0	12.6	10.65	9.5	12.8	11.03	96.57
A.L. 400-1a	9.8	11.2	10.48	9.8	11.2	10.48	100.0
A.L. 417-1a	8.9	10.8	9.80	8.6	11.2	9.81	99.90
L.H. 3	12.6	10.6	11.56	11.1	11.7	11.40	**101.40**
L.H. 4	10.6	10.0	10.30	10.3	10.7	10.50	98.10
L.H. 14	10.3	10.7	10.50	10.9	11.5	11.20	93.75
EP 2400/00	10.8	10.0	10.39	9.1	11.4	10.19	**101.96**
MAK-VP-1/12	9.7	9.5	9.60	9.7	10.8	10.24	93.75
KSD-VP-1/39	10.1	8.4	9.21	11.3	9.0	10.08	91.37
MKM-VP-1/626	10.9	10.7	10.80	11.0	11.7	11.34	95.24
LDD-VP-1/672[b]	8.4	9.5	8.93	9.5	9.2	9.35	95.51

[a] P_3 area/P_4 area × 100. Ratios in bold indicate that the P_3 crown area is larger than the P_4 crown area.
[b] The MD value of the P_4 is corrected for wear and/or damage (Melillo et al., 2021).

molars are generally more expanded buccolingually even though the M_2 of MSD-VP-5/16 falls within the range of the species (Fig. 19). Compared to *Au. anamensis*, and *Au. afarensis*, the overall size of the teeth in MSD-VP-5/16 and MSD-VP-5/50 falls within the range of variation documented for both species (Fig. 19). In *Au. anamensis* specimens retaining both premolars, the P_3 crown area is larger than the P_4 area in 4 of 5 specimens. In *Au. afarensis* specimens, the P_3 crown area is larger than the P_4 crown area only in 5 of 18 specimens (Table 4). In MSD-VP-5/50, the P_3 crown area is larger than the P_4 (Fig. 19; Table 4). In terms of molar proportions, *Ar. ramidus* has an M_3 with crown area that is on average slightly smaller than the M_2. There is substantial amount of overlap in the sizes of the M_2s and M_3s of both *Au. anamensis* and *Au. afarensis* (Fig. 19). In some specimens, the M_2s are larger than the M_3s, whereas in others, the M_3s are larger than the M_2s. The M_3 of MSD-VP-5/50 is larger than the M_2 (Fig. 19). In terms of the crown outline of the M_3, it tends to taper distally in *Ar. ramidus*. Some *Au. anamensis* and *Au. afarensis* M_3s also show similar distal tapering. MSD-VP-5/50 approaches some *Ar. ramidus* M_3s in terms of its distal tapering (e.g., ARA-VP-6/500). The dental sample size of *Au. deyiremeda* is currently limited to only one of each postcanine tooth (BRT-VP-3/14). The occlusal area of both premolars in this specimen is smaller than MSD-VP-5/16 and MSD-VP-5/50 (Fig. 19). The P_3 in BRT-VP-3/14 also has one of the smallest mesiodistal dimensions in the comparative sample. However, the crown area of its M_1 and M_2 are larger than the M_1 and M_2 of both MSD mandibles while its M_3 is slightly smaller than that of MSD-VP-5/50 but within the range of both *Au. anamensis* and *Au. afarensis* (Fig. 19).

4. Discussion

Comparisons with mandibles and teeth of *Ar. ramidus*, *Au. anamensis*, *Au. afarensis* (Laetoli + Hadar), and *Au. deyiremeda* indicate that the MSD mandibles from Woranso-Mille cannot be definitively assigned to any one of these species per se. However, their overall morphology warrants their assignment to *Australopithecus*. The Woranso-Mille mandibles lack dentognathic features that are autapomorphic to *Ar. ramidus* (e.g., single-rooted P_4, a trait seen in all known P_4s of the species known from Middle Awash and Gona; Suwa et al., 2009a; Semaw et al., 2005). They lack a relatively small M_1, extremely inflated mandibular corpus, and anteriorly positioned ramus root—diagnostic features described for *Au. deyiremeda* (Haile-Selassie et al., 2015).

Each of the Woranso-Mille mandibles variably retains some mandibular and dental features that distinguish *Au. anamensis* from *Au. afarensis* (see Ward et al., 2001, 2020). This is also the case with other 3.8–3.6 Ma hominins from Woranso-Mille (Haile-Selassie et al., 2010b). The Allia Bay sample of *Au. anamensis* shows dentognathic features that are relatively more derived toward *Au. afarensis* (e.g., the presence of metaconid in the P_3 of KNM-ER 20432). If the two Woranso-Mille mandibles described here were included in the Allia Bay hypodigm of *Au. anamensis*, the differences would not exceed the normal range of variation expected in a population of a single species. The same applies to their assignment to *Au. afarensis* even though they would substantially increase the amount of variation in mandibular corpus and dental arcade shape in the species. The one comparable adult *Au. afarensis* mandible from Laetoli (L.H. 4) shares few primitive features with *Au. anamensis* (Kimbel et al., 2006; Harrison, 2011). However, the Woranso-Mille mandibles share with *Au. anamensis* some mandibular features that are absent in L.H. 4 (e.g., the anterior to posterior corpus transition being at C_1 in MSD-VP-5/16, more inclined external contour of the symphysis and much lower mandibular corpus shape index in MSD-VP-5/50). The P_3s of *Au. afarensis* from Laetoli also have well-developed metaconids, which characterize most P_3s of all later hominins. In terms of corpus shape, however, L.H. 29 from Laetoli has an absolutely deeper jaw (at M_2 = 38.4 mm)

compared to all of the Hadar *Au. afarensis* mandibles ($n = 16$; mean = 32.6 ± 4.1 mm; range = 25.3–37.6 mm; Harrison, 2011) but MSD-VP-5/50 is still deeper with 44.9 mm at M_2.

The dentognathic morphology and metrics of the Woranso-Mille mandibles could be expected in late *Au. anamensis*, or early *Au. afarensis*, and the dental morphological differences between the two specimens could be accommodated within the expected range of variation in a single species. Both Woranso-Mille mandibles lack the full suite of dentognathic features that are diagnostic of *Au. anamensis* from the type site while they retain some features of this species that are absent in *Au. afarensis* from Laetoli and Hadar. Based on this, one could argue that they are best assigned to *Au. anamensis*. The presence of *Au. anamensis* at Woranso-Mille in deposits that are dated to 3.8 Ma would also lend support to this assignment. On the other hand, they share some derived dentognathic features (incipient metaconid in the P_3 of MSD-VP-5/50 and less retreating external symphyseal contour in MSD-VP-5/16) with *Au. afarensis* and it could be equally argued that their assignment to *Au. afarensis* is more parsimonious and the mandibular features that they share with Kanapoi *Au. anamensis* are symplesiomorphies with no taxonomic significance. However, these symplesiomorphies are also mainly the features that distinguish *Au. anamensis* from *Au. afarensis* (e.g., P_3 and symphyseal morphology, dental arcade shape). Therefore, it is difficult to convincingly assign the two ca. 3.76 Ma Woranso-Mille mandibles to either *Au. anamensis* or *Au. afarensis* at this time and further analysis will be needed with more dentognathic material from the 4.1–3.8 Ma period in order to understand temporal trends in the dentognathic morphology of the *Au. anamensis–Au. afarensis* chronospecies lineage. However, regardless of which *Australopithecus* species they belong to, they are extremely important in further supporting the hypothesized ancestor–descendant relationship between *Au. anamensis* and *Au. afarensis* because they retain a mosaic of dentognathic morphology that is present in both species.

5. Conclusions

Hominin fossils from Woranso-Mille, dated to between 3.8 and 3.6 Ma, have played a crucial role in addressing some outstanding questions in hominin evolution during the Pliocene. One of these questions is related to the hypothesized ancestor–descendant relationship between *Au. anamensis* and *Au. afarensis*. In the present study, we have presented a comparative description of two ca. 3.76 Ma hominin mandibles that are relevant to addressing this question. These mandibles show metric and morphological similarities with both *Au. anamensis* and *Au. afarensis*. Both mandibles variably retain mandibular morphological features that are present only in the *Au. anamensis* sample from Kanapoi even though they lack the full suite of dentognathic traits that are diagnostic of the species. They also share a few derived dentognathic features with *Au. afarensis* from both Laetoli and Hadar, making their definitive assignment to either species difficult. However, the presence of *Au. anamensis* at Woranso-Mille in 3.8 Ma deposits increases the likelihood of their assignment to *Au. anamensis*. Regardless of which species they are assigned to, the mosaic nature of the dentognathic morphology and geological age of the two mandibles lend further support to the hypothesized ancestor–descendant relationship between *Au. anamensis* and *Au. afarensis*. However, there is now limited fossil evidence indicating that these two species may have overlapped in time. *Australopithecus afarensis* was possibly present at Laetoli, Tanzania, as early as 3.8 Ma, about the same time as *Au. anamensis* (MRD cranium) at Woranso-Mille. Recent studies have also shown that the 3.9 Ma Belohdelie frontal from the Middle Awash might also belong to *Au. afarensis*. Hence, the last appearance of *Au. anamensis* and first appearance of *Au. afarensis* remains unknown. Recovery of *Australopithecus* fossils from 4.1 to 3.8 Ma is thus critical to further address the timing of these events.

Declaration of competing interest

We declare that we have no known competing financial interests or personal relationships that could have appeared to influence the work reported in this paper.

Acknowledgments

This research was supported by the Cleveland Museum of Natural History, earlier grants from the US National Science Foundation (BCS-1124705, BCS-1124713, BCS-1124716, BCS-1125157, and BCS-1125345), the National Geographic Society, and The Leakey Foundation. We thank the Authority for Research and Conservation of Cultural Heritage (ARCCH) of the Ethiopian Ministry of Culture and Tourism for permission to conduct field research at Woranso-Mille and laboratory work in the National Museum of Ethiopia in Addis Ababa; the government of the Afar Regional State for administrative support; the Afar people of the Woranso-Mille area and the Mille District administration for their hospitality and support; and field crew members of the Woranso-Mille Paleontological Research Project. For access to original fossil specimens in their care we also thank D. Dagne, Y. Assefa, M. Endalamaw, T. Getachew, G. Tekle, S. Melaku, and the National Museum of Ethiopia; F.K. Manthi and the National Museums of Kenya; and B. Zipfel and the Evolutionary Studies Institute at the University of the Witwatersrand. We are also grateful to the Casting Lab technicians in the Paleoanthropology Laboratory of ARCCH. We thank T.M. Ryan and T. Stecko at the Center for Quantitative Imaging, Pennsylvania State University, for CT scanning and image processing, A. Jaeger for surface scanning, and A. Ragni for help with R Statistics. We are grateful to B. Asfaw, the late W.H. Kimbel, G. Suwa, and T. White, for sharing unpublished data, and to W.H. Kimbel for constructive comments, edits, and discussions, C. Dean for discussions about dental development, and D. Su and S. Melillo for edits and assistance with some figures. We are grateful to Andrea Taylor, the Associate Editor, and four anonymous reviewers for constructive comments and edits that considerably improved this manuscript.

References

Alemseged, Z., Wynn, J.G., Kimbel, W.H., Reed, D., Geraads, D., Bobe, R., 2005. A new hominin from the Basal Member of the Hadar Formation, Dikika, Ethiopia, and its geological context. J. Hum. Evol. 49, 499–514.

Alemseged, Z., Spoor, F., Kimbel, W.H., Bobe, R., Geraads, D., Reed, D., Wynn, J.G., 2006. A juvenile early hominin skeleton from Dikika, Ethiopia. Nature 443, 296–301.

Alemseged, Z., Wynn, J.G., Geraads, D., Reed, D., Barr, W.A., Bobe, R., McPherron, S.P., Deino, A., Alene, M., Sier, M.J., Roman, D., Mohan, J., 2020. Fossils from Mille-Logya, Afar, Ethiopia, elucidate the link between Pliocene environmental changes and *Homo* origins. Nat. Commun. 11, 2480.

Berger, L.R., de Ruiter, D.J., Churchill, S.E., Schmid, P., Carlson, K.J., Dirks, P.H.G.M., Kibii, J.M., 2010. *Australopithecus sediba*: A new species of *Homo*-like australopith from South Africa. Science 328, 195–204.

Berger, L.R., Hawks, J., de Ruiter, D.J., Churchill, S.E., Schmid, P., Delezene, L.K., Kivell, T.L., Garvin, H.M., Williams, S.A., DeSilva, J.M., Skinner, M.M., Musiba, C.M., Cameron, N., Holliday, T.W., Hartcourt-Smith, W., Ackermann, R.R., Bastir, M., Bogin, B., Bolter, D., Brophy, J., Cofran, Z.D., Congdon, K.A., Deane, A.S., Dembo, M., Drapeau, M., Elliott, M.C., Feuerriegel, E.M., Garcia-Martinez, D., Green, D.J., Gurtov, A., Irish, J.D., Kruger, A., Laird, M.F., Marchi, D., Meyer, M.R., Nalla, S., Negash, E.W., Orr, C.M., Radovcic, D., Schroeder, L., Scott, J.E., Throckmorton, Z., Tocheri, M.W., VanSickle, C., Walker, C.S., Wei, P., Zipfel, B., 2015. *Homo naledi*, a new species of the genus *Homo* from the Dinaledi Chamber, South Africa. Elife 4, e09560.

Brown, F.H., McDougall, I., Gathogo, P.N., 2013. Age ranges of *Australopithecus* species, Kenya, Ethiopia, and Tanzania. In: Reed, K.E., Fleagle, J.G., Leakey, R.E. (Eds.), The Paleobiology of *Australopithecus*. Springer, Dordrecht, pp. 7–20.

Brunet, M., Beauvilain, A., Coppens, Y., Heintz, E., Moutaye, A.H.E., Pilbeam, D., 1996. *Australopithecus bahrelghazali*, une nouvelle espèce d'Hominidé ancien de la région de Koro Toro (Tchad). C. R. Acad. Sci. 322, 907–913.

Brunet, M., Guy, F., Pilbeam, D., Mackaye, H.T., Likius, A., Ahounta, D., Beauvilain, A., Blondel, C., Bocherens, H., Boisserie, J.-R., De Bonis, L., Coppens, Y., Dejax, J., Denys, C., Duringer, P., Eisenmann, V., Fanone, G., Fronty, P., Geraads, D., Lehmann, T., Lihoreau, F., Louchart, A., Mahamat, A., Merceron, G., Mouchelin, G., Otero, O., Campomanes, P.P., Ponce De Leon, M., Rage, J.-C., Sapanet, M., Schuster, M., Sudre, J., Tassy, P., Valentin, X., Vignaud, P., Viriot, L., Zazzo, A., Zollikofer, C., 2002. A new hominind from the Upper Miocene of Chad, Central Africa. Nature 418, 145–151.

Campisano, C.J., Feibel, C.S., 2007. Connecting local environmental sequences to global climate patterns: Evidence from the hominin-bearing Hadar Formation, Ethiopia. J. Hum. Evol. 53, 515–527.

Campisano, C.J., Feibel, C.S., 2008. Tephrostratigraphy of the Hadar and Busidima Formations at Hadar, Afar Depression, Ethiopia. In: Quade, J., Wynn, J.G. (Eds.), The Geology of Early Humans in the Horn of Africa, Geological Society of America Special Paper 446, Boulder, Colorado, pp. 135–162.

Chamberlain, A.T., Wood, B.A., 1985. A reappraisal of variation in hominid mandibular corpus dimensions. Am. J. Phys. Anthropol. 66, 399–405.

Curran, S.C., Haile-Selassie, Y., 2016. Paleoecological reconstruction of hominin-bearing middle Pliocene localities at Woranso-Mille. J. Hum. Evol. 96, 97–112.

Dean, C., Zanolli, C., Le Cabec, A., Tawane, M., Garrevoet, J., Mazurier, A., Macchiarelli, R., 2020. Growth and development of the third permanent molar in *Paranthropus robustus* from Swartkrans, South Africa. Sci. Rep. 10, 19053.

Deino, A.L., Scott, G.R., Saylor, B., Alene, M., Angelini, J.D., Haile-Selassie, Y., 2010. $^{40}Ar/^{39}Ar$ dating, paleomagnetism, and tephrochemistry of Pliocene strata of the hominid bearing Woranso-Mille area, west-central Afar Rift, Ethiopia. J. Hum. Evol. 58, 111–126.

Delezene, L.K., Kimbel, W.H., 2011. Evolution of the mandibular third premolar crown in early *Australopithecus*. J. Hum. Evol. 60, 711–730.

Delezene, L.K., Zolnierz, M.S., Teaford, M.F., Kimbel, W.H., Grine, F.E., Ungar, P.S., 2013. Premolar microwear and tooth use in *Australopithecus afarensis*. J. Hum. Evol. 65, 282–293.

DiMaggio, E.N., Campisano, C.J., Rowan, J., Dupont-Nivet, G., Deino, A.L., Bibi, F., Lewis, M.E., Souron, A., Garello, D., Werdelin, L., Reed, K.E., Arrowsmith, A., 2015. Late Pliocene fossiliferous sedimentary record and the environmental context of early *Homo* from Afar, Ethiopia. Science 347, 1355–1359.

Glowacka, H., Kimbel, W.H., Johanson, D.C., 2017. Aspects of mandibular ontogeny in *Australopithecus afarensis*. In: Marom, A., Hovers, E. (Eds.), Human Paleontology and Prehistory. Springer, Cham, pp. 127–144.

Guy, F., Mackaye, H.T., Likius, A., Vignaud, P., Schmittbuhl, M., Brunet, M., 2008. Symphyseal shape variation in extant and fossil hominoids, and the symphysis of *Australopithecus bahrelghazali*. J. Hum. Evol. 55, 37–47.

Haile-Selassie, Y., 2010. Phylogeny of early *Australopithecus*: New fossil evidence from the Woranso-Mille (central Afar, Ethiopia). Philos. Trans. R. Soc. Lond. B Biol. Sci. 365, 3323–3331.

Haile-Selassie, Y., Ryan, T.M., 2019. Comparative description and taxonomy of new hominin juvenile mandibles from the Pliocene of Woranso-Mille (Central Afar, Ethiopia). J. Hum. Evol. 132, 15–31.

Haile-Selassie, Y., Latimer, B.M., Alene, M., Deino, A.L., Gibert, L., Melillo, S.M., Saylor, B.Z., Scott, G.R., Lovejoy, C.O., 2010a. An early *Australopithecus afarensis* postcranium from Woranso-Mille, Ethiopia. Proc. Natl. Acad. Sci. USA 107, 12121–12126.

Haile-Selassie, Y., Saylor, B.Z., Deino, A., Alene, M., Latimer, B.M., 2010b. New hominid fossils from Woranso-Mille (Central Afar, Ethiopia) and taxonomy of early *Australopithecus*. Am. J. Phys. Anthropol. 141, 406–417.

Haile-Selassie, Y., Saylor, B.Z., Deino, A., Levin, N.E., Alene, M., Latimer, B.M., 2012. A new hominin foot from Ethiopia shows multiple Pliocene bipedal adaptations. Nature 483, 565–569.

Haile-Selassie, Y., Gibert, L., Melillo, S.M., Ryan, T.M., Alene, M., Deino, A., Levin, N.E., Scott, G., Saylor, B.Z., 2015. New species from Ethiopia further expands Middle Pliocene hominin diversity. Nature 521, 483–488.

Haile-Selassie, Y., Melillo, S.M., Su, D.F., 2016a. The Pliocene hominin diversity conundrum: Do more fossils mean less clarity? Proc. Natl. Acad. Sci. USA 113, 6364–6371.

Haile-Selassie, Y., Melillo, S.M., Ryan, T.M., Levin, N.E., Saylor, B.Z., Deino, A., Mundil, R., Scott, G., Mulugeta, A., Gibert, L., 2016b. Dentognathic remains of *Australopithecus afarensis* from Nefuraytu (Woranso-Mille, Ethiopia): Comparative description, geology, and paleoecological context. J. Hum. Evol. 100, 35–53.

Haile-Selassie, Y., Melillo, S.M., Vazzana, A., Benazzi, S., Ryan, T.M., 2019. A 3.8-million-year-old hominin cranium from Woranso-Mille, Ethiopia. Nature 573, 214–219.

Harrison, T., 2011. Hominins from the Upper Laetolil and Upper Ndolanya Beds, Laetoli. In: Harrison, T. (Ed.), Paleontology and Geology of Laetoli: Human Evolution in Context. Springer, Dordrecht, pp. 141–188.

Herries, A.I.R., Martin, J.M., Leece, A.B., Adams, J.W., Boschian, G., Joannes-Boyau, R., Edwards, T.R., Mallett, T., Massey, J., Murszewski, A., Neubauer, S., Pickering, R., Strait, D.S., Armstrong, B.J., Baker, S., Caruana, M.V., Denham, T., Hellstrom, J., Moggi-Cecchi, J., Mokobane, S., Penzo-Kajewski, P., Rovinsky, D.S., Schwartz, G.T., Stammers, R.C., Wilson, C., Woodhead, J., Menter, C., 2020. Contemporaneity of *Australopithecus*, *Paranthropus*, and early *Homo erectus* in South Africa. Science 368, eaaw7293.

Johanson, D.C., White, T.D., 1979. A systematic assessment of early African hominids. Science 203, 321–330.

Johanson, D.C., White, T.D., Coppens, Y., 1978. A new species of the genus *Australopithecus* (Primates: Hominidae) from the Pliocene of Eastern Africa. Kirtlandia 28, 1–14.

Johanson, D.C., White, T.D., Coppens, Y., 1982. Dental remains from the Hadar Formation, Ethiopia: 1974–1977 collections. Am. J. Phys. Anthropol. 57, 545–603.

Kimbel, W.H., Delezene, L.K., 2009. "Lucy" redux: A review of research on *Australopithecus afarensis*. Am. J. Phys. Anthropol. 140, 2–48.

Kimbel, W.H., Rak, Y., Johanson, D.C., 2004. The Skull of *Australopithecus afarensis*. Oxford University Press, Oxford.

Kimbel, W.H., Lockwood, C.A., Ward, C.V., Leakey, M.G., Rak, Y., Johanson, D.C., 2006. Was *Australopithecus anamensis* ancestral to *A. afarensis*? A case of anagenesis in the hominin fossil record. J. Hum. Evol. 51, 134–152.

Leakey, M.D., 1987. The Laetoli hominid remains. In: Leakey, M.D., Harris, J.M. (Eds.), Laetoli: A Pliocene Site in Northern Tanzania. Clarendon, Oxford, pp. 108–117.

Leakey, M.G., Feibel, C.S., McDougall, I., Walker, A., 1995. New four-million-year-old hominid species from Kanapoi and Allia Bay, Kenya. Nature 376, 565–571.

Leakey, M.G., Feibel, C.S., McDougall, I., Ward, C., Walker, A., 1998. New specimens and confirmation of an early age for *Australopithecus anamensis*. Nature 393, 62–66.

Leakey, M.G., Spoor, F., Brown, F.H., Gathogo, P.N., Kiarie, C., Leakey, L.N., McDougall, I., 2001. New hominin genus from eastern Africa shows diverse middle Pliocene lineages. Nature 410, 433–440.

Lockwood, C.A., Kimbel, W.H., Johanson, D.C., 2000. Temporal trends and metric variation in the mandibles and dentition of *Australopithecus afarensis*. J. Hum. Evol. 39, 23–55.

Melillo, S.M., Gibert, L., Saylor, B.Z., Deino, A., Alene, M., Ryan, T.M., Haile-Selassie, Y., 2021. New Pliocene hominin remains from Leado Dido'a area of Woranso-Mille, Ethiopia. J. Hum. Evol. 153, 102956.

Moggi-Cecchi, J., Menter, C., Boccone, S., Keyser, A., 2010. Early hominin dental remains from the Plio-Pleistocene site of Drimolen, South Africa. J. Hum. Evol. 58, 374–405.

Rak, Y., Ginzburg, A., Geffen, E., 2007. Gorilla-like anatomy on *Australopithecus afarensis* mandibles suggests *Au. afarensis* link to robust australopiths. Proc. Natl. Acad. Sci. USA 104, 6568–6572.

Saylor, B.Z., Angelini, J., Deino, A., Alene, M., Fournelle, J.H., Haile-Selassie, Y., 2016. Tephrostratigraphy of the Waki-Mille area of the Woranso-Mille paleoanthropological research project, Afar, Ethiopia. J. Hum. Evol. 93, 25–45.

Saylor, B.Z., Gibert, L., Deino, A., Alene, M., Levin, N.E., Melillo, S.M., Peaple, M.D., Feakins, S.J., Bourel, B., Barboni, D., Novello, A., Sylvestre, F., Mertzman, S.A., Haile-Selassie, Y., 2019. Age and context of mid-Pliocene hominin cranium from Woranso-Mille, Ethiopia. Nature 573, 220–224.

Semaw, S., Simpson, S.W., Quade, J., Renne, P.R., Butler, R.F., McIntosh, W.C., Levin, N., Dominguez-Rodrigo, M., Rogers, M.J., 2005. Early Pliocene hominids from Gona, Ethiopia. Nature 433, 301–305.

Spoor, F., Leakey, M.G., Leakey, L.N., 2010. Hominin diversity in the Middle Pliocene of eastern Africa: The maxilla of KNM-WT 40000. Philos. Trans. R. Soc. Lond. B Biol. Sci. 365, 3377–3388.

Spoor, F., Leakey, M.G., O'Higgins, P., 2016. Middle Pliocene hominin diversity: *Australopithecus deyiremeda* and *Kenyanthropus platyops*. Philos. Trans. R. Soc. Lond. B Biol. Sci. 371, e1–e9.

Strait, D.S., Grine, F.E., Moniz, M.A., 1997. A reappraisal of early hominid phylogeny. J. Hum. Evol. 32, 17–82.

Strait, D.S., Grine, F.E., 2004. Inferring hominoid and early hominid phylogeny using craniodental characters: The role of fossil taxa. J. Hum. Evol. 47, 399–452.

Su, D., Haile-Selassie, Y., 2022. Mosaic habitats at Woranso-Mille (Ethiopia) during the Pliocene and implications for *Australopithecus* paleoecology and taxonomic diversity. J. Hum. Evol. 163, 103076.

Suwa, G., Kono, R.T., Simpson, S.W., Asfaw, B., Lovejoy, C.O., White, T.D., 2009a. Paleobiological implications of the *Ardipithecus ramidus* dentition. Science 326, 94–99.

Suwa, G., Asfaw, B., Kono, R.T., Kubo, D., Lovejoy, C.O., White, T.D., 2009b. The *Ardipithecus ramidus* skull and its implications for hominind origins. Science 326, 68e1–68e7.

Villmoare, B., Kimbel, W.H., Seyoum, C., Campisano, C.J., DiMaggio, E.N., Rowan, J., Braun, D.R., Arrowsmith, J.R., Reed, K.E., 2015. Early *Homo* at 2.8 Ma from Ledi-Geraru, Afar, Ethiopia. Science 347, 1352–1355.

Ward, C.V., Leakey, M.G., Walker, A., 2001. Morphology of *Australopithecus anamensis* from Kanapoi and Allia Bay, Kenya. J. Hum. Evol. 41, 255–368.

Ward, C.V., Manthi, F.K., Plavcan, J.M., 2013. New fossils of *Australopithecus anamensis* from Kanapoi, West Turkana, Kenya (2003-2008). J. Hum. Evol. 65, 501–524.

Ward, C.V., Plavcan, J.M., Manthi, F.K., 2020. New fossils of *Australopithecus anamensis* from Kanapoi, West Turkana, Kenya (2012-2015). J. Hum. Evol. 140, 102368.

White, T.D., 1977. New fossil hominids from Laetolil, Tanzania. Am. J. Phys. Anthropol. 46, 197–229.

White, T.D., 1980. Additional fossil hominids from Laetoli, Tanzania: 1976-1979 specimens. Am. J. Phys. Anthropol. 53, 487–504.

White, T.D., 2003. Early hominids – Diversity or distortion? Science 299, 1994–1997.

White, T.D., Johanson, D.C., 1982. Pliocene hominid mandibles from the Hadar Formation, Ethiopia: 1974-1977 collections. Am. J. Phys. Anthropol. 57, 501–544.

White, T.D., Suwa, G., Asfaw, B., 1994. *Australopithecus ramidus*, a new species of early hominid from Aramis, Ethiopia. Nature 371, 306–312.

White, T.D., Suwa, G., Simpson, S.W., Asfaw, B., 2000. Jaws and teeth of *Australopithecus afarensis* from Maka, Middle Awash, Ethiopia. Am. J. Phys. Anthropol. 111, 45–68.

White, T.D., WoldeGabriel, G., Asfaw, B., Ambrose, S., Beyene, Y., Bernor, R.L., Boisserie, J.-R., Currie, B., Gilbert, W.H., Haile-Selassie, Y., Hart, W.K., Hlusko, L.J., Howell, F.C., Kono, R.T., Lehmann, T., Louchart, A., Lovejoy, O.C., Renne, P.R., Saegusa, H., Vrba, E.S., Wesselman, H., Suwa, G., 2006. Asa Issie, Aramis and the origin of *Australopithecus*. Nature 440, 883–889.

White, T.D., Asfaw, B., Beyene, Y., Haile-Selassie, Y., Lovejoy, O.C., Suwa, G., WoldeGabriel, G., 2009. *Ardipithecus ramidus* and the paleobiology of early hominids. Science 326, 75–86.

White, T.D., Lovejoy, O.C., Asfaw, B., Suwa, G., 2015. Neither chimpanzee nor human, *Ardipithecus* reveals the surprising ancestry of both. Proc. Natl. Acad. Sci. USA 112, 4877–4884.

Wood, B., Boyle, E.K., 2016. Hominin taxic diversity: Fact or fantasy? Yrbk. Phys. Anthropol. 159, S37–S78.